Nutrient-deprived growth of streptomycetes reveals a novel growth phenotype with enhanced antimicrobial activity

Niklas Söderholm[a,b], Hugh Tanner[a,b], Linda Sandblad[a,b*#]

[a]Department of Chemistry, Umeå University, 901 87 Umeå, Sweden

[b]The Laboratory for Molecular Infection Medicine Sweden (MIMS), 901 87 Umeå, Sweden

Address correspondence to Linda Sandblad, linda.sandblad@umu.se

Abstract

The capacity of gram-positive streptomycetes to adapt to various environments is reflected in the sheer size of their genomes and the number of encoded regulatory proteins. However, typical studies of Streptomycetes are conducted using media rich in available nutrients. Here, we demonstrate that *S. coelicolor* colonies respond to nutrient depletion with a phenotype transition. We refer to this phenotype as "foraging growth" for its submerged and continuous growth on depleted media. The foraging phenotype differ distinctly from colonies on nutrient-rich media, in terms of colony morphology, genomic stability and their secretome. The results demonstrate that adaption to nutrient deprivation through foraging is found throughout the phylogeny, indicating it is highly conserved. Furthermore, foraging *S. coelicolor* gains the ability to inhibit mold on deprived media and exhibits an altered metabolomic profile. An enhanced competitive activity against gram-negative and gram-positive bacteria was also observed among the tested species. These findings highlight the morphological adaptions of streptomycetes during nutrient deprived growth and demonstrate altered secondary metabolite production and that novel antimicrobial activities can be detected.

Introduction

The gram-positive genus *Streptomyces*, known for its filamentous morphology and production of bioactive secondary metabolites, plays a crucial role in soil as saprophytes hydrolyzing a wide array of polysaccharides and macromolecules (Chater, Biro, Lee, Palmer, & Schrempf, 2010). Streptomycetes undergo a complex life cycle, beginning with spore germination, progressing through vegetative hyphal growth and branching to form a mycelial network. A differentiation process leads to the development of aerial hyphae and spores, which often coincide with activation of secondary metabolites. The differentiation relies on the *bld*-genes to control aerial development and the *whi*-genes for spore maturation (McCormick & Flardh, 2012). The life cycle of streptomycetes has

46 extensively been studied on rich media where subsequent nutrient depletion is thought to contribute
47 to mycelial differentiation and secondary metabolite production.
48
49 While the importance of optimized growth medium for metabolite production and life cycle
50 progression is widely recognized, few have examined nutrient poor conditions. The abundance of gene
51 regulatory proteins, two-component systems, transporters, and substrate-binding proteins identified
52 in the *S. coelicolor* genome suggests a significant capacity for adaptation and the utilization of varied
53 nutrient sources (Bentley et al., 2002; Nikolaidis et al., 2023). A recent study on rich media showed
54 that *S. coelicolor* metabolite production was enhanced because of genomic heterogeneity (Z. Zhang
55 et al., 2020). Additionally, certain streptomycetes exhibit an “exploratory phenotype" when co-
56 incubated with yeast or by specific media components alone (S. E. Jones et al., 2017; Shepherdson &
57 Elliot, 2022). As for conventional growth, exploratory growth is closely connected to metabolite
58 production and activates cryptic metabolites (Shepherdson & Elliot, 2022).
59
60 Genetic identification of biosynthetic gene clusters (BGCs) has revealed that each *Streptomyces spp.*
61 could have the capacity to produce over 20 secondary metabolites (Bentley et al., 2002; Ikeda et al.,
62 2003; Ohnishi et al., 2008; Qin et al., 2017). However, standard cultivation often fails to stimulate the
63 activation of the regulatory pathways responsible for their synthesis (Nett, Ikeda, & Moore, 2009; Ochi
64 & Hosaka, 2013). After exhausting primary substrates, carbon catabolite repression enables the
65 adaptation of growth and metabolism to utilize to less prioritized substrates. Rapidly consumed
66 carbon sources are often found to repress production of secondary metabolites (Romero-Rodriguez
67 et al., 2017). Therefore, altering environmental stimuli to activate silent secondary metabolite
68 production is a promising strategy in the search for new bioactive compounds (X. Zhang, Hindra, &
69 Elliot, 2019).
70

71 In this study, we demonstrate that global nutrient depletion in growth media coincides with a
72 morphological transition of *S. coelicolor* colonies to a phenotype termed "foraging". Our findings
73 reveal that *bldA* is not essential for foraging growth, although TTA codon-containing gene products
74 were detected in the foraging secretome. Additionally, *S. coelicolor* exhibited mold-inhibitory activity
75 under nutrient-depleted conditions. Metabolomic analysis showed significant changes in the
76 metabolome, and growth inhibition assays suggested roles for *bldA* and *adpA* in antimicrobial activity
77 during nutrient-deprived growth. These results underscore a competitive advantage for foraging
78 colonies on nutrient-deprived media. Furthermore, all strains cultured under these conditions
79 exhibited foraging growth, suggesting this behavior is evolutionarily conserved. This study indicates
80 that nutrient-deprived growth may be a key method to both generate novel bioactive secondary
81 metabolites in addition to providing a more complete understanding of the life cycle.
82

83 ## Results

84 **Phenotype transition from conventional *S. coelicolor* colony morphology correlate with**
85 **nutrient depletion.**

86 In a phenotypic screening of different media formulation, we observed a unique growth morphology
87 of *S. coelicolor* after 60 days on 0.5x diluted TSA medium. The colonies had developed an unusual
88 thinner, veil-like, outer growth zone, distinct from the conventional *S. coelicolor* morphology (Fig. 1A).
89 This morphology, termed "foraging growth", was further investigated using time-lapse imaging over
90 75 days and revealed a morphological transition around day 50 (Video S1).
91

92 This transition appears linked to nutrient availability, as it occurred earlier on smaller media volumes
93 and later on undiluted TSA. Foraging growth was evident already after 21 days when grown in ⌀ 4 cm
94 dishes with 0.5xTSA. Using these dishes, we monitored nutrient depletion by inoculating plates with
95 spores and sampled the agar every three days for 27 days and analyzed nutrient content using mass

96 spectrometry. Samples were taken 0.5 cm away from the colony, to ensure that the samples would
97 not be contaminated with hyphae, and the very edge of the dish. Altogether, 51 metabolites were
98 annotated, including sugars, amino acids, and fatty acids, most of which depleted over time (Fig. 1B).
99 Nutrient levels proximal to the colony mirrored those at the dish-edge (Figure 1 – figure supplement
100 1A). Although the levels of e.g., glucose and fructose were depleted at foraging onset, others e.g.,
101 levels of glutamine and lactic acid initially increased before decreasing. Some, e.g., leucine and
102 phenylalanine, remained stable until day 12, before decreasing (Fig. 1C, Figure 1 – figure supplement
103 1B). The levels of some, e.g., sucrose, stayed constant throughout, and only five metabolites increased
104 more than one-fold (Fig. 1C). However, supplementing these metabolites in 0.5xTSA and MS agar did
105 not induce foraging growth. These findings demonstrate that the morphological transition coincides
106 with media nutrient depletion.
107

108 **Nutrient depletion promotes foraging growth.**

109 Modified *Streptomyces*-minimal medium only contain two carbon sources: agar and 55 mM glucose
110 (Kieser et al., 2000). Observing that foraging growth commenced upon carbon source depletion, we
111 excluded glucose, making agar the sole carbon source in the modified medium, hereafter referred to
112 as foraging agar media (FAM). Colonies on FAM displayed similar characteristics to those on 0.5xTSA
113 post-transition, exhibiting a thin, veil-like submerged expansion eventually covering the entire plate
114 (Fig. 2A). Over time, lineages developed within the colony, some of which became pigmented (Fig.
115 2B). The amount of aerial hyphae and pigment production at the inoculation site was influenced by
116 the presence of metabolizable nutrients, such as glycerol, in the spore storage buffer (Fig. 2C),
117 underscoring the effect of nutrients on the growth characteristics of the foraging phenotype. FAM
118 supplemented with glucose or fructose effectively inhibited foraging growth, leading to conventional
119 raised colonies (Fig. 2D). Notably, sucrose supplementation of FAM did not prevent foraging growth,
120 indicating the inability of *S. coelicolor* to metabolize sucrose.

121

122 Time-lapse imaging captured the progressive expansion and sector formation of a foraging colony on
123 FAM (Fig. 2E, Supplementary Video S2). Introduction of glucose or tryptone to a foraging colony
124 induced raised colony growth and strong pigment production, typical for growth in nutrient-rich
125 conditions (Fig. 2F, 2G, Supplementary Video S3 and S4). Scanning Electron Microscopy (SEM) imaging
126 of FAM revealed predominantly submerged hyphal growth, with limited hyphae at the surface (Fig.
127 2H). Aerial hyphae were found both at the site of inoculation and uncommonly at other patches
128 throughout the colony. In contrast, growth on nutrient-rich media such as 0.5x TSA revealed that
129 vegetative hyphae were primarily piled up on the surface, with only a few extending further into the
130 agar.

131

132 Sector formation was observed during foraging growth (Fig. 1, 2A, 2B, Video S1 and S2). To investigate
133 these sectors for potential genomic instability as reported for *S. coelicolor* grown on nutrient rich
134 media (Z. Zhang et al., 2020), a lineage from the initial inoculation, a subsequent sector 'A', and its
135 subsequent sectors 'I' and 'IV', were sequenced using the Illumnia platform. Analysis using breseq
136 software (Deatherage & Barrick, 2014) showed no significant genomic instability compared to growth
137 on nutrient-rich media. Only three mutations were identified: two mutations in sector A, in the
138 chromosomal replication initiator protein DnaA (SCO3879, E520K) and in a hypothetical protein
139 (SCO1511, Q8CK26). Sector IV had an additional mutation in a putative regulator (SCO5582, Q9ZBP7)
140 (Figure 2 – figure supplement 1). These mutations did not visibly affect colony morphology on rich
141 media. Altogether, these results demonstrate that *S. coelicolor* behaves distinctly during nutrient
142 deprived growth.

143

144 ***S. coelicolor* foraging growth secretome is both Sec and Tat dependent.**

145 *S. coelicolor* grown on a deprived media such as FAM must utilize the agar as the main carbon source.
146 Agar degradation was visualized by staining the plates with iodine-based Lugol's solution, which
147 revealed a distinct halo around the colonies indicating substrate degradation (Fig. 3A). Proteins were
148 extracted from the zones outside of foraging colonies and analyzed using mass spectrometry. The
149 resulting protein composition was visualized using proteomaps (Liebermeister et al., 2014). Of the 203
150 detected proteins, 52 were annotated into six categories: membrane transport, biosynthesis, central
151 carbon metabolism, signal transduction, other enzymes, and
152 folding/sorting/degradation/transcription, as shown in the treemap (Fig. 3B) and the proteins
153 represented in the gene name mosaic map (Fig. 3C).
154
155 Signal peptide prediction on all *S. coelicolor* coding sequences using SignalP 6.0 (Teufel et al., 2022)
156 identified 696 proteins with signal sequences. Prediction of the 203 proteins in the foraging secretome
157 showed: 56 with the Sec translocon, 18 with the Tat translocon and 123 without any signal peptide
158 (Fig. 3D, Supplementary table S1). Proteomaps of these three groups indicated functional overlaps
159 among proteins with Sec, Tat and without signal peptides (Fig. 3E). Comparing our findings with
160 previous studies of *S. coelicolor* secretomes on rich media (Kim, Chater, Lee, & Hesketh, 2005; Widdick
161 et al., 2006) showed that 24% of the proteins identified in foraging conditions were also detected in
162 nutrient-rich conditions, while 75% were unique to foraging, including the glucose-repressible
163 extracellular agarose DagA (Figure 3 – figure supplement 1A, Supplementary table S2). Comparing the
164 proteins lacking signal peptides from foraging (n=203) and rich conditions (n=401) revealed an overlap
165 of 60 proteins (Supplementary table S4).
166
167 PANTHER classification of signal peptide-containing proteins categorized them into four groups (Fig.
168 3F, Supplementary table S4). Notably, the transporter category included the ABC transporter BldKB,
169 known for its role in carbon catabolite repression and mycelium formation (Chavez et al., 2011;
170 Nodwell & Losick, 1998). The metabolite interconversion category featured 13 hydrolases and one

171 oxidoreductase, while the protein modifying enzyme category included ten proteases and a ubiquitin-
172 protein ligase. Among the unclassified proteins were additional hydrolases and solute binding
173 proteins. The non-signal peptide proteins were classified into 11 categories (Figure 3 – figure
174 supplement 1B, Supplementary table S5).
175
176 Four proteins in the foraging secretome, encoded by genes containing the *bldA*-specific TTA codon,
177 suggest that *bldA* is active during foraging growth: an uncharacterized protein without a signal peptide
178 (Q9L2F9, SCO2524), a carbohydrate-binding module (CBM) domain-containing hydrolase (Q9RKF0,
179 SCO3487) with a Sec-signal peptide, and two uncharacterized secreted proteins with Sec-signal
180 peptides (Q9RKE0, SCO3498 and Q9K452, SCO7233) (Supplementary table S6). In total, 24 secretome
181 proteins identified in the Carbohydrate-Active enZYmes (CAZy) Database (Drula et al., 2022) are
182 associated with hydrolytic and non-hydrolytic cleavage of glycosidic bond and carbohydrate adhesion
183 (FIG 3G).
184
185 In summary, these results uncover the secretome components crucial for foraging growth of *S.*
186 *coelicolor* on depleted media, highlighting the role of both Sec and Tat transport systems in nutrient
187 degradation and uptake of agar components.
188
189 **Foraging phenotype is found across the phylogeny of *Streptomyces*.**
190 To investigate the influence of classical developmental regulators (*bld* and *whi*) on foraging growth,
191 we cultured wild-types and developmental-mutants on FAM and found that all tested mutants
192 displayed the foraging phenotype (Figure 4 – figure supplement 1A). Notably, the *bldA* mutant
193 exhibited foraging growth despite the presence of TTA-codon containing gene products in the foraging
194 secretome.
195

We then extended the study to various *Streptomyces spp.*, representing different branches of the phylogenetic tree (Table 1), to assess if foraging growth was unique to *S. coelicolor*. Pairwise average nucleotide identity (ANI) values were utilized to create a heatmap that groups strains according to their genomic similarity, showing that only *S. coelicolor* and *S. lividans* shared an ANI >99 (Fig. 4A). All tested strains displayed the foraging growth phenotype on FAM (Fig. 4B), with little to no pigmentation and agar degradation confirmed by Lugol's solution staining (Figure 4 – figure supplement 1B). Similar to *S. coelicolor*, the foraging growth was inhibited in all strains with the addition of 1% glucose or tryptone to FAM (Figure 4 – figure supplement 1C and 1D). Additionally, from local soil samples grown on FAM, we selected seven colonies exhibiting the foraging morphology. These were all confirmed to be *Streptomyces* spp. using MALDI-TOF analysis (Supplementary table S7). This observation suggests the ubiquity of foraging growth across the Streptomycetes phylogenetic spectrum. Furthermore, the growth behavior of developmental mutants on FAM indicates that these traditional developmental regulators do not control foraging growth.

Table 1. Phylogenetic clades of *streptomycetes* according to Labeda *et al.*, 2012.

Species	Clade
S. antibioticus	4
S. filipiniensis	10
S. griseus	*
S. anulatus	*
S. griseolus	36
S. venezuelae	40
S. kanamyceticus	*
S. noursei	67
S. hygroscopicus	75
S. hiroshimensis	84
S. coelicolor	112
S. lividans	**
K. setae	***

* Unsupported and single member clusters

** Not included in Labeda *et al.*, 2012

*** Clusters outside of Streptomyces according to Labeda *et al.*, 2017

214

215 **Foraging *S. coelicolor* displays an altered metabolomic profile.**

216 *S. coelicolor* colonies grown on FAM were found to inhibit the growth of a contaminating mold (Fig.
217 5A), identified as *Penicillium citrinum* through 18S/ITS sequencing. This inhibition was replicated by
218 growing *S. coelicolor* on FAM for five days before inoculating *P. citrinum* spores at a distance of 2 cm,
219 resulting in an average 4.3 mm inhibition zone (±0.76 mm, n = 96). Inhibition was not observed when
220 glucose was added to the agar or on any other nutrient-rich media, nor on FAM with pH below 7.
221 Interestingly, the *bldA* mutant, is typically unable to produce certain antimicrobial metabolites,
222 inhibited *P. citrinum* growth on FAM. However, the *adpA*-mutant strain M851 showed less inhibition
223 compared to the wild-type (Fig. 5B). All tested *whi*-mutants (-A, -B, -G, -H, and -I) exhibited mold-
224 inhibitory activity (Figure 5 – figure supplement 1A). Inhibition of a local *Aspergillus spp*. isolate was
225 also demonstrated using an overlay assay with a 100x diluted TSA-overlay, since the *Aspergillus spp.*
226 did not grow on FAM (Figure 5 – figure supplement 1B). However, no inhibition of *Saccharomyces*
227 *cerevisiae* or *Candida albicans* was detected using the same assay.

228

229 To explore the metabolomic profile of *S. coelicolor* grown on FAM and FAM supplemented with 1%
230 glucose (FAM+G), agar was sampled around the colonies for mass spectrometric analysis. The
231 metabolomic profiles differed between FAM and FAM+G, both in negative (R2(X)=0.75, Q2(X)=0.97)
232 and positive detection modes (R2(X)=0.63, Q2(X)=0.47) (Fig. 5C, 5E). Some features with relatively
233 higher concentrations on FAM-agar (highlighted in green in Fig. 5D, 5F) could be matched with known
234 *S. coelicolor* metabolites based on monoisotopic molecular weight using the StreptomeDB
235 (Moumbock et al., 2021). Among these annotated features, the signaling molecule γ-butyrolactone
236 was found at higher concentrations in FAM+G. Wailupemycin G was the only annotated metabolite
237 found at considerably higher concentrations on FAM+G (Fig. 5G, Table 2). There were 30 features,
238 with higher levels in the FAM condition, that could not be annotated using their monoisotopic mass

and StreptomeDB (Supplementary table S8). Twelve of these features were unique to FAM and not detected in any other tested condition (Figure 5 – figure supplement 1C and 1D).

The mass spectrometry results demonstrate a significant alteration in the metabolomic profile of foraging *S. coelicolor*. The mold inhibitory assay using mutants suggests that mold inhibition involves *adpA* and other genes dependent on *bldA*.

Table 2 Metabolomic features annotated using monoisotopic mass and StreptomeDB.

Annotation	Detection mode/RT	ppm error
7-Acetyl-3.6-dihydroxy-8-methyl-tetralone	+/3.44	3.4
7-Acetyl-3.6-dihydroxy-8-methyl-tetralone	-/3.03	0.9
Acetylglucosamine	+/0.39	0.3
Aloesaponarin II	+/3.16	0.4
Dehydromutacin	+/3.26	1.9
Fluostatin C	+/3.06	1.2
Fluostatin C	+/3.38	1.2
Fluostatin C	+/7.27	7.4
Fluostatin F	+/3.93	0.1
Fluostatin K	+/3.16	1.5
γ-butyrolactone	-/1.42	2.6
Gentisic acid	-/3.76	2.5
Homogentisic acid / Orsellic acid	-/2.02	1.5
Litmomycin	+/2.85	1.5
Mycothiol	+/1.14	12.5
Tryptophan	-/2.26	0.6
Wailupemycin G	+/0.4	11.2

*RT = Retention time

Foraging *Streptomycetes* demonstrate increased antibacterial activity.

To investigate whether mold-inhibition was a common behavior during foraging, all *Streptomyces spp.* tested for foraging growth above, were tested for mold inhibition. However, none of the other species

252 inhibited *P. citrinum*. The altered metabolome of *S. coelicolor* during foraging, combined with its ability
253 to hinder mold growth, led us to investigate its potential to inhibit bacterial growth. Due to the
254 nutrient-depleted state of FAM, *B. subtilis* and *E. coli* were unable to proliferate. Therefore, to test for
255 antibacterial activity, we overlaid FAM with foraging *S. coelicolor* colonies with diluted LA and then
256 added *B. subtilis* 168 and *E. coli* MG1655 on top of the LA layers. The growth was evaluated after
257 incubation using a stereo microscope. This method was applied to all previously studied *Streptomyces*
258 *spp.* to assess their antibacterial properties. Most species showed increased inhibitory activity on
259 nutrient-depleted FAM-agar compared to FAM supplemented with glucose (FAM+G) and tryptone
260 (FAM+T) (Fig. 6A). However, *S. coelicolor* did not exhibit enhanced antibacterial activity on FAM
261 compared to the nutrient-supplemented media.
262
263 Analysis of bacterial inhibition by developmental mutants indicated that the *bldA*-mutant lost its
264 ability to inhibit *B. subtilis* growth, whereas the *adpA* mutant acquired the ability to inhibit *E. coli* (Fig.
265 6B). In summary, these findings suggest that streptomycetes are more competitive on FAM than on
266 rich agar. The distinct responses of the *bldA* and *adpA* mutants further emphasize their roles in the
267 antimicrobial activities of foraging *S. coelicolor*.
268

269 ## Methods

270 **Strains, media, and culture conditions**

271 The strains used in this study are listed in Supplementary Table S9. Streptomyces strains were grown
272 on FAM (1 g $(NH_4)_2SO_4$, 0.5 g $K_2PO_4x7H_2O$, 0.1 g $FeSO_4x7H_2O$, 10 g agar, in 1L pH 7.5) (Kieser et al.,
273 2000). FAM were supplemented with 1% of various sugars: glucose (FAM+G), sucrose (FAM+S),
274 fructose (FAM+F) or tryptone as an amino acid source (FAM+T) when indicated. To investigate the
275 effect of pH on mold-inhibition the pH of FAM was set using HEPES-buffer and HCl/NaOH. Tryptone
276 soy broth (Thermo Fisher Scientific) was prepared according to instructions and diluted 0.5x when

277 indicated with water and 1.5% agar added before autoclaving. MS-agar (20 g mannitol, 20 g Soy flour,
278 15 g agar in 1L) agar were used for sporulation and petri dish time-lapse imaging. Effects of
279 accumulated metabolites were conducted by adding 20mg/ml: beta-alanine, meso-erythriol (Merck),
280 Potassium-citramalate monohydrate (Merck), urea (Merck), and pantothenic acid (Merck). All
281 incubations were carried out at 30°C.

282 **Isolation and identification of local isolates**

283 The inhibited mold was isolated from the FAM dish and recultivated on TSA. The agar plate was sent
284 to Eurofins for 18S/ITS sequencing. For isolation of local streptomycetes, soil samples from potatoes
285 and plant soil were dried at room temperature before being deposited on FAM. The plates were
286 incubated at 37°C until foraging colonies were observed after approx. 5–10 days. Colonies with
287 characteristic foraging phenotypes were re-streaked on TSA and characterized using MALDI-TOF
288 (Bruker). The local *Aspergillus spp.* was isolated from a soil sample and assessed morphologically.

289 **Colony imaging**

290 For all imaging of small colonies spores were inoculated on agar media and visualized using a Nikon
291 SMZ1500 dissection microscope and a Nikon Digital sight DS-Fi1 camera, with either surface
292 illumination using LEDs or oblique sub-stage illumination. Whole petri dishes were imagined using a
293 Nikon D7000 DSLR. Agar time-lapses were recorded using a Raspberry Pi 3 model B with camera
294 module v2 mounted in a 10x lens (Olympus). The device was placed in a 30°C dark room with an LED
295 lamp programmed to illuminate the plate only during image capture, one frame per hour. ImageJ
296 distribution Fiji (Schindelin et al., 2012) was used to process single frames into videos and Adobe
297 Photoshop CC software for still images.

298 **Electron microscopy**

299 Colonies of *S. coelicolor* on agar were cut, fixed overnight at 4°C in 2.5% glutaraldehyde/0.1M sodium
300 cacodylate buffer, dehydrated in series of ethanol, critical point dried and coated with a 5 nm Au/Pd

301 before being analyzed with a Merlin Field Emission SEM (Zeiss) using SE-HE2 and in-lens detectors.
302 Images were processed using Adobe Photoshop CC software.

303 **Inhibition assays**

304 For mold inhibition, *Streptomyces* spores were inoculated on FAM and incubated at 30°C for 5 days.
305 Spores from *P. citrinum* were inoculated 2 cm from the foraging colony. The plates were incubated for
306 14 days and observed daily for inhibition zones and imaged as described above. For bacterial
307 inhibition, plates with *Streptomyces spp.* were incubated for 20 days before a thin layer of 100x diluted
308 TSA (1.5% agar) was placed on top of agar and incubated overnight at 4°C. Overnight cultures of *E. coli*
309 and *B. subtilis* were diluted and $2x10^7$ CFU in 100 µl was added to the agar overlays and incubated
310 overnight at 37°C. Inhibition zones were assessed and imaged using a Nikon SMZ1500 dissection
311 microscope and a Nikon Digital sight DS-Fi1 camera.

312 **Foraging secretome protein analysis**

313 The agar outside of foraging *S. coelicolor* on FAM incubated for 20 days was extracted. The agar was
314 crushed and incubated overnight with water in a 50 ml Falcon tube. Proteins in the supernatant were
315 precipitated by addition of TCA and incubated on ice of 4 minutes before centrifugation at 20,000g for
316 5 min. The pellet was washed twice with 200 µl ice-cold acetone. The pellet was dried, dissolved in
317 protein sample buffer and loaded on an SDS-PAGE. Protein dense regions were cut and sent for mass
318 spectroscopy identification to Linköping University, where general in-gel digestion was performed as
319 described by Shevchenko *et al.* (Shevchenko, Tomas, Havlis, Olsen, & Mann, 2006).

320 **Metabolomic analysis**

321 Metabolic profiling of media nutrients by GC-MS was performed at the Swedish Metabolomics Center
322 in Umeå, Sweden. For the nutrient analysis of agar, six replicates of agar plugs were collected from
323 the edge of the dish and 0.5 cm away from the *S. coelicolor* colonies on 0.5xTSA medium. This sampling
324 was performed on six different ⌀ 4 cm plates. Three control samples were taken at every time point

325 from three sterile 0.5xTSA dishes. Sample preparation was performed according to A *et al.* (A et al.,
326 2005). The samples were stored at -80 °C until analysis. Small aliquots of the remaining supernatants
327 were pooled and used to create quality control (QC) samples. The samples were analyzed in batches
328 according to a randomized run order on GC-MS. Derivatization and GCMS analysis were performed as
329 described previously A *et al*. (A et al., 2005). Non-processed MS-files from the metabolic analysis were
330 exported from the ChromaTOF software in NetCDF format to MATLAB-R2020a (Mathworks, Natick,
331 MA, USA), where all data pre-treatment procedures (base-line correction, chromatogram alignment,
332 data compression and Multivariate Curve Resolution) were performed. The extracted mass spectra
333 were identified by comparisons of their retention index and mass spectra with libraries of retention
334 time indices and mass spectra (Schauer et al., 2005). Mass spectra and retention index comparison
335 was performed using NIST MS 2.2 software. Annotation of mass spectra was based on reverse and
336 forward searches in the library. Masses and ratio between masses indicative of a derivatized
337 metabolite were especially notified. The mass spectrum with the highest probability indicative of a
338 metabolite and the retention index between the sample and library for the suggested metabolite was
339 ± 5 the deconvoluted "peak" was annotated as an identification of a metabolite. The annotated
340 nutrients were plotted using GraphPad Prism (version 9.0.2) to show trends over time and ridge plots
341 were generated using R version 4.2 and packages ggplot2 3.4.4 and ggridges 0.5.4.

342 For untargeted metabolite analysis, agar stubs were punched out from just outside of *S. coelicolor*
343 colonies on FAM and FAM+G. For each condition, twelve samples were isolated from plates inoculated
344 with *S. coelicolor*, in addition to two control samples each from sterile plates. The weight of the
345 samples were adjusted to 100 mg before the addition of 1 mL extraction buffer (90/10 v/v
346 methanol:water). Internal standards (13C9-Phenylalanine, 13C3-Caffeine was, D4-Cholic acid, D8-
347 Arachidonic Acid, 13C9-Caffeic Acid) were added to each sample. The sample was shaken at 30 Hz for
348 3 min in a mixer mill, and proteins were precipitated at +4 °C for 2h on ice. The sample was centrifuged
349 at +4 °C, 14 000 rpm, for 10 min. The supernatant was transferred to a microvial and solvents
350 evaporated. Before analysis, the sample was re-suspended in 10 + 10 µL methanol and water. The set

351 of samples were analyzed in positive mode and negative mode. The chromatographic separation was
352 performed on an Agilent 1290 Infinity UHPLC-system (Agilent Technologies, Waldbronn, Germany).
353 Re-suspended aliquots (2 µL) of the agar extracts were injected onto an Acquity UPLC HSS T3, 2.1 x 50
354 mm, 1.8 µm C18 column in combination with a 2.1 mm x 5 mm, 1.8 µm VanGuard precolumn (Waters
355 Corporation, Milford, MA, USA) held at 40°C. The gradient elution buffers were A (H2O, 0.1 % formic
356 acid) and B (75/25 acetonitrile:2-propanol, 0.1 % formic acid). The compounds were detected with an
357 Agilent 6550 Q-TOF mass spectrometer equipped with a jet stream electrospray ion source. The
358 settings were kept identical between the modes, except the capillary voltage. The data processing was
359 performed using the Recursive Feature Extraction algorithm within Agilent Masshunter Profinder
360 version B.08.00 (Agilent Technologies Inc., Santa Clara, CA, USA). All multivariate statistical
361 investigations (PCA) were performed using the software package SIMCA®-P+ version 15.0.2 (Umetrics,
362 Umeå, Sweden). Annotation of unknown metabolites were performed by comparing monoisotopic
363 molecular weights with *S. coelicolor* metabolites in the StreptomeDB (Moumbock et al., 2021) using R
364 software (4.2). Metabolomic features were plotted using GraphPad Prism (version 9.0.2). All raw mass
365 spectrometry files used in this study have been deposited to ScieLifeLab Data Repository with the
366 dataset identifier DOI: https://doi.org/10.17044/scilifelab.c.7171122.

367 **Average nucleotide identity of streptomycetes**

368 FastANI (Jain, Rodriguez, Phillippy, Konstantinidis, & Aluru, 2018) version 1.33 was employed to
369 calculate the Average Nucleotide Identity (ANI) values, assessing the genomic similarity among the 13
370 species investigated in this study (GenBank assembly IDs: GCA_000010605.1, GCA_000203835.1,
371 GCA_000269985.1, GCA_000721185.1, GCA_000739105.1, GCA_001514065.1, GCA_001886595.1,
372 GCA_008704495.1, GCA_014649495.1, GCA_014650335.1, GCA_016917755.1, GCA_019933235.1,
373 GCA_020783455.1), were analyzed using FastANI with its default settings. Pairwise comparisons were
374 conducted across all genomes, and the resulting ANI values were utilized to generate a heatmap using
375 R version 4.2.

376 **DNA sequencing of foraging sectors**

377 Two levels of sectors formed during foraging on FAM were grown in TSB-media and 600 mg of pellet
378 was sent to MicrobesNG for Illumnia sequencing. Quality controlled and trimmed reads with 30x
379 coverage were obtained and analyzed using breseq software (Deatherage & Barrick, 2014) with
380 default settings, using the S. coelicolor A(3)2 reference genome (Genbank: GCA_000203835.1,
381 (Bentley et al., 2002)) updated using wild-type sequence data to accommodate for genomic variation
382 in lab strain. The reads of descendent sectors were mapped against this updated reference genome.
383 Illumnia read data used in this study have been deposited to SciLifeLab Data Respository with the
384 dataset identifier DOI: https://doi.org/10.17044/scilifelab.c.7171122.

385 **Statistical analysis**

386 In this study, certain measurements in the untargeted metabolomics analysis fell below the detection
387 limits, resulting in missing values. To ensure an accurate representation of our findings and maintain
388 the integrity of the statistical analysis, these missing values were omitted from the dataset.
389 Consequently, all values presented in the violin plots depict observable data trends and variations
390 above the detection threshold. All statistical analyses were conducted using GraphPad Prism (version
391 9.0.2). Details on the specific type of statistical analysis and the criteria for significance testing are
392 provided in the legends of the respective figures.

393 Discussion

394 The primary habitat of streptomycetes, the soil, is a dynamic environment with variable
395 environmental factors. Laboratory cultivation on a narrow range of rich media may not fully represent
396 adaptations occurring in the diverse, competitive soil environment. This study reports a novel
397 phenotype-transition of *S. coelicolor* colonies upon nutrient depletion.

398

399 Metabolomics analysis showed that the phenotype transition on 0.5xTSA coincided with nutrient
400 depletion, leading to the "foraging phenotype". Media composition is known to be crucial for life-cycle
401 progression, with nutrient depletion often referred to as the trigger of differentiation and sporulation,
402 though the process is acknowledged to be complex (Barka et al., 2016; Bush, Tschowri, Schlimpert,
403 Flardh, & Buttner, 2015; Flardh & Buttner, 2009; McCormick & Flardh, 2012). Instead of a sporulation,
404 *S. coelicolor* responded to nutrient depletion with a phenotype transition. Four distinct trends in
405 metabolite dynamics were distinguishable: depletion, accumulation, initial accumulation followed by
406 depletion, and unchanged levels. The trend of initial accumulation followed by depletion is likely due
407 to the breakdown of macromolecules in the TSA-media. It is established that fluctuations of
408 metabolite levels during growth are a result of the breakdown and uptake of external sources and
409 subsequent release into the surroundings (Douglas, 2020). Steady accumulation may occur from by-
410 product export or independently of metabolite overflow (Pinu et al., 2018). Supplementation of the
411 accumulated metabolites to media did not trigger foraging growth, suggesting they do not act as
412 signals for phenotype transition. However, two accumulated metabolites, β-alanine and pantothenic
413 acid, are crucial in various biochemical pathways. β-alanine, essential for pantothenic acid synthesis –
414 a precursor of Coenzyme A – enhances respiration in alkaline soils (Datta et al., 2017). Their release
415 might influence the microbial landscape in the natural habitat of *S. coelicolor*.
416
417 Nutrient levels proximal to the colony and at the edge of the dish closely followed each other,
418 explaining the persistence of the foraging phenotype even as it expands into unexplored areas.
419 Calculations based on agar diffusion coefficients suggest that nutrients like glucose can diffuse 1.5 cm^2
420 over three days (Miyamoto, Atsuyama, Ekino, & Shin, 2018).
421
422 In contrast to rich media, where low molecular weight organic compounds are abundant (Kieser et al.,
423 2000; Shirling & Gottlieb, 1966), soil environments typically have transient availability of such
424 nutrients (D. L. Jones & Murphy, 2007; Rousk & Jones, 2010). The amount of complex carbohydrates

425 and plant debris of fertile soils are considered high, but there is also a flux of available nutrients
426 throughout the year that the soil inhabitants need to accommodate for (Randewig, Marshall,
427 Näsholm, & Jämtgård, 2019). FAM, our minimal defined agar medium without glucose, supports spore
428 germination and foraging growth, but growth reverted to conventional phenotype upon the addition
429 of nutrients. This indicates that the complex polysaccharides in agar are not preferred over simpler
430 organic compounds. Nitrogen and phosphate also play a crucial role in cycle progression and
431 metabolite production. Our FAM media, with higher nitrogen levels than typically found in soil, may
432 influence these processes (Rousk & Jones, 2010). Nitrogen-concentrations higher than 1 mM allow
433 synthesis of glutamate independent of ATP, but low levels require the activity of glutamate synthetase
434 (Reuther & Wohlleben, 2007). Glutamate synthetase II activity its mRNA levels correlate with mycelial
435 differentiation on solid media demonstrating its importance in mycelial development (Fink,
436 Weissschuh, Reuther, Wohlleben, & Engels, 2002). High levels of nitrogen in rich media cause
437 repression of secondary metabolite production (Hodgson, 2000). Further, high levels of inorganic
438 phosphate have been shown to inhibit the production of several secondary metabolites (Bibb, 2005;
439 Hobbs et al., 1992; Martin, 2004). Accordingly, we detected an increase of some metabolites during
440 FAM-growth, but we also detected a decreased production of several metabolites. Microdiffusion
441 experiments in soils have revealed that there is a significant flux of organic nitrogen (Inselsbacher &
442 Nasholm, 2012; Inselsbacher, Öhlund, Jämtgård, Huss-Danell, & Näsholm, 2011; Leitner et al., 2017).
443 A nitrogen source in the form of organic ammonium, as e.g., asparagine prevents foraging growth on
444 FAM-plates. It will therefore be of future interest to evaluate the effect of altered nitrogen and
445 phosphate levels as well as organic versus inorganic sources, on foraging growth and metabolome.
446
447 The foraging secretome contained 74 proteins with predicted signal peptides. Comparing the foraging
448 secretome with rich growth secretome (Widdick et al., 2006) showed that 75% of foraging secretome
449 was not found during rich growth. This underscores the adaptation that takes place upon nutrient
450 depletion that results in the foraging phenotype. Despite the presence of *bldA*-dependent proteins in

451 the secretome, a *bldA*-mutant still displayed foraging growth, suggesting *bldA*-regulation is not
452 essential for this phenotype. The developmental protein BldKB was identified in the secretome,
453 suggesting a role in foraging. Additionally, the foraging behavior was observed in various *Streptomyces*
454 species, indicating it may be a common feature across the genus (Labeda et al., 2017; Labeda et al.,
455 2012). Multi locus sequence analysis suggests that *Kitasatospora* is a distinct genus, and suggests that
456 foraging is not limited to *Streptomycetes*, since foraging growth was also observed for *K. setae*.
457
458 The study demonstrates that foraging growth conditions affect secondary metabolism. The gained
459 ability of *S. coelicolor* to inhibit mold-growth together with the overall enhanced potential of other
460 *Streptomyces spp*. to inhibit gram-positive and gram-negative bacteria suggests that there are also
461 significant alterations of their metabolomes. This shows potential for using FAM growth in screening
462 for active secondary metabolites not produced on rich media. However, the low nutrient levels used
463 for the overlay assays could also influence the target bacteria rendering them more susceptible to the
464 antimicrobial effects of foraging colonies. It is well established that growth conditions, e.g., choice of
465 carbon source, affect secondary metabolism of streptomycetes (Sanchez et al., 2010; van Keulen &
466 Dyson, 2014) and other strategies are also being employed to activate silent BGC (Ochi & Hosaka,
467 2013; van der Meij, Worsley, Hutchings, & van Wezel, 2017). A recent discovery shows that secondary
468 metabolite production is significantly increased as a result from genetic instability on nutrient rich MS-
469 agar (Z. Zhang et al., 2020). We could however not find any support for major mutational deletions
470 during foraging growth when investigating the sectors formed during foraging growth. This further
471 emphasizes that the survival strategies of *S. coelicolor* differ between depleted and rich growth
472 conditions.
473
474 The mechanism by which foraging growth is regulated remains to be elucidated. Identifying the
475 regulatory components would result in understanding the required nutrient deprived conditions.
476 Importantly, knowledge about its regulation could also be utilized as a tool for manipulating the

477 production of the secondary metabolites. In summary, this study demonstrates that nutrient-deprived
478 growth leads to a distinct growth phenotype and altered metabolome, with enhanced antimicrobial
479 properties. This novel growth behavior and its metabolic implications offer new insights into
480 environmental adaptation and competitiveness of streptomycetes under nutrient deprivation with
481 potential implications in anti-microbial drug discovery.
482

483 ## Additional files

484 - Figure 1 – figure supplement 1. Nutrient levels during phenotype transition on 0.5xTSA.
485 - Figure 2 – figure supplement 1. Sector mutations of foraging colonies.
486 - Figure 3 – figure supplement 1. Secretome of foraging colonies.
487 - Figure 4 – figure supplement 1. Growth of *Streptomyces spp.* on FAM.
488 - Figure 5 – figure supplement 1. Mold inhibition and unannotated metabolomic features.
489 - Supplementary table 1. Prediction of signal peptides in the foraging secretome using SignalP
490 6.0.
491 - Supplementary table 2. Comparison of the foraging secretome with proteins secreted on rich
492 media (Widdick et al 2006).
493 - Supplementary table 3. Comparison of cytosolic protein detected during foraging growth and
494 growth on rich media by Widdick et al (2006).
495 - Supplementary table 4. PANTHER classification of signal peptide containing proteins with
496 regard to protein class.
497 - Supplementary table 5. PANTHER classification of cytosolic protein with regard to protein
498 class.
499 - Supplementary table 6. TTA containing genes in *S. coelicolor* A3(2).
500 - Supplementary table 7. Locally isolates streptomcyetes.

501 • Supplementary table 8. Monoisotopic mass of features significantly higher levels in FAM
502 conditions.
503 • Supplementary table 9. Strain list.
504 • Video 1. *S. coelicolor* phenotype transition.
505 • Video 2. *S. coelicolor* growing on FAM-agar.
506 • Video 3. Addition of glucose to foraging *S. coelicolor.*
507 • Video 4. Addition of tryptone to foraging *S. coelicolor.*
508 • Figure 1 - source data 1. Nutrient fold change values over time used for the ridge plots.
509 • Figure 1 – source data 2. Nutrient fold change values for edge and proximal samples used for
510 plotting single nutrients over time.
511 • Figure 1 – figure supplement 1B – source data. Nutrient fold change values for edge and
512 proximal samples used for plotting single nutrients over time.
513 • Figure 4A – source data. ANI values for each species used for generating the heatmap.
514 • Figure 5G – source data. Values used for plotting the annotated features detected using
515 untargeted mass spectrometry.
516 • Figure 5 – figure supplement 1D – source data. Values used for plotting the unannotated
517 features specific to foraging growth on FAM detected using untargeted mass spectrometry.
518

519 ## Data availability

520 The Illumina sequencing data and the metabolomics mass spectrometry data has been deposited in
521 the SciLifeLab Data Repository under DOI: https://doi.org/10.17044/scilifelab.c.7171122
522
523 The following datasets were generated
524 Sandblad, Linda; Söderholm, Niklas (2024). Foraging growth of Streptomyces - Datasets. SciLifeLab.
525 Collection. https://doi.org/10.17044/scilifelab.c.7171122

Acknowledgments

We thank National Microscopy Infrastructure, NMI (VR-RFI 2016-00968) at Umeå Centre for Electron Microscopy (UCEM). Swedish Metabolomics Centre, Umeå, Sweden (www.swedishmetabolomicscentre.se) is acknowledged for metabolic profiling by LC-MS and GC-MS. Illumnia sequencing was provided by MicrobesNG (http://www.microbesng.com). Postdoc fellowship funding from the Kempe foundations and Sven och Lilly Lawskis foundation. Project granted by Umeå Centre for Microbial research (UCMR) and Swedish Foundation for Strategic Research (RIF21-0067). Anders Sjöstedt for MALDI-TOF analysis of streptomycetes and Ala Javadi for sample preparation.

Figure legends

Figure 1. *S. coelicolor* growth phenotype transition correlates with nutrient depletion. (**A**) Colony appearance after 75 days growth on 0.5xTSA. The point of phenotype transition is indicated by the dotted circle. (**B**) Visualization comparing nutrient levels during *S. coelicolor* growth on 0.5xTSA. The distribution within each ridge plot shows the variation in fold change across the time points. The amplitude of each peak indicates how common the fold changes are for that nutrient. Each nutrient is accompanied by a colored square indicating its status at the end of the time series. The measurements proximal to the colony were taken in sextuplicate for each time point and normalized against the controls. Source file of all fold change over time used for the ridge plots is available in the Figure 1 – Source data 1. (**C**) Examples of metabolites levels throughout the study. The time point where the transition to foraging growth was observed is indicated with the dotted lines on day 21. Each measurement proximal to the colony and at the edge of the dish were taken in sextuplicate for each time point and normalized against the controls. Source file of nutrient fold change over time in edge and proximal samples used for the plots is available in the Figure 1 – Source data 2.

550 **Figure 2.** Nutrient poor agar media promote the *S. coelicolor* foraging phenotype. (**A**) *S. coelicolor*
551 spores in glycerol storage buffer inoculated on FAM. The foraging phenotype covering the petri dish
552 was photographed after 15 weeks of incubation at 30°C. Transparent pigment-free and lightly
553 pigmented sectors are visible. (**B**) A photograph of a pigmented sector extending towards the edge of
554 the dish. (**C**) Formation of aerial hyphae were only observed at the site of spore inoculation. (**C**) A
555 photograph of aerial hyphae at the site of spore inoculation. (**D**) Micrograph showing the phenotypic
556 growth on WT *S. coelicolor* inoculated on FAM, FAM+sucrose (+S), FAM+glucose (+G) and
557 FAM+fructose (+F) for 15 weeks at 30°C. (**E**) Time-lapse stills showing the foraging growth progression
558 at day 12, 26, 40, 52. (**F**) Time-lapse stills after addition of glucose (+G) to a foraging colony at day 0,
559 4, 8, 12. (**G**) Time-lapse stills of addition of tryptone (+T) to a foraging colony. (**H**) SEM imaging of *S.*
560 *coelicolor* grown on FAM and 0.5xTSA for 7 days. The glycerol storage buffer was washed away and
561 replaced with water. A top view of the center of the colonies and at the edge show few hyphae at the
562 surface of the FAM. Hyphae extending through the agar are mainly observed on the FAM-plates, while
563 they predominantly grow on top on 0.5xTSA.

564 **Figure 3.** Characterization of the foraging phenotype secretome. (**A**) Micrograph of foraging *S.*
565 *coelicolor* grown on FAM, stained with lugol solution. (**B**) Treemap displaying the functional categories
566 of subproteomes from the foraging secretome. Out of 203 detected proteins, 52 were assigned to
567 categories. The category area size represents the number of assigned proteins in each category, not
568 protein abundance. (**C**) Mosaic showing the gene names within each category. Area size does not
569 represent protein abundance. (**D**) Number of proteins containing a signal sequence in the foraging
570 secretome, predicted using SignalP 6.0 (Teufel et al., 2022). Categories include general secretory (Sec)
571 substrates cleaved by SPase I (Sec/SPI) or SPase II (Sec/SPII, lipoproteins) and twin-arginine substrates
572 cleaved by SPase I (Tat/SPI) or SPase II (Tat/SPII, lipoprotein), and "No SP" for no predicted signal
573 peptide. (**E**) Treemap showing the functional categories when separated into the groups: No SP (left,
574 22/129 proteins assigned), Sec (middle, 17/56 proteins assigned) and Tat-signal peptide (right, 7/18
575 proteins assigned). (**F**) PANTHER functional classification of proteins from the foraging secretome with

576 predicted signal peptides. The graph shows the number of proteins assigned to each protein class. (**G**)
577 CAZy classification of the foraging secretome: Glycoside Hydrolases (GH), Polysaccharide Lyases (PLs)
578 and Carbohydrate-Binding Modules (CBMs).

579 **Figure 4.** Phylogenetically separated streptomycetes display the foraging phenotype. (**A**) Heatmap
580 visualizing pairwise ANI values, calculated using fastANI (Jain et al., 2018), among the genomes of
581 tested species as a quantitative measure of their genomic similarity. Each cell in the heatmap
582 represents the ANI percentage between a pair of genomes. The branches of a dendrogram represent
583 how each strain is grouped based on hierarchical clustering with euclidean distance as the metric for
584 dissimilarity. Source file of ANI values used for the heatmap is available in the Figure 4 – Source data
585 1. (**B**) Microscopy images showing the foraging phenotype of each *Streptomyces spp.* cultivated for
586 three weeks on FAM. Abbreviations: SANT; *S. antibioticus*, SANU; *S. anulatus*, SCO; *S. coelicolor*, SFI;
587 *S. filipinensis*, SGR; *S. griseus*, SGRI; *S. griseolus*, SHIR; *S. hiroshimensis*, SHYG; *S. hygroscopicus*, SKAN;
588 *S. kanamyceticus*, SLIV; *S. lividans*, SNOR; *S. norsei*, SVEN; *S. venezuelae*, KSET; *Kitasatospora setae*.

589 **Figure 5.** Mold inhibitory activity and metabolomic analysis of foraging *S. coelicolor*. (**A**) Inhibition
590 zones around *S. coelicolor* on FAM contaminated by *P. citrinum* mold. (**B**) Inhibition zones around *S.*
591 *coelicolor* wild-type (WT), bldA and M851 (*adpA*-mutant) inoculated with *P. citrinum*. (**C**) Scores plot
592 of LC-MS analysis in negative detection mode of FAM and FAM+G-agar inoculated with *S. coelicolor*.
593 (**D**) Loadings plot from negative detection mode. Features with relatively elevated levels on FAM are
594 highlighted in blue and features with relatively elevated levels in FAM+G-agar are highlighted in red.
595 (**E**) Scores plot of LC-MS analysis in positive detection mode of FAM and FAM+G-agar inoculated with
596 *S. coelicolor*. (**F**) Loadings plot from positive detection mode. Features with relatively elevated levels
597 on FAM-agar are highlighted in blue and features with relatively elevated levels in FAM+G-agar are
598 highlighted in red. (**G**) Graphs showing the features annotated by monoisotopic mass and
599 StreptomeDB. All graphs depict statistically significant outcomes comparing FAM and FAM+G as
600 determined by t-tests, with p-values <=0.0002. 7-Acetyl-3.6-dihydroxy-8-methyl-tetralone is

601 abbreviated as 7A36D8MT in the plot. Source file with plotted values is available in the Figure 5 –
602 Source data 1.

603 **Figure 6.** Antibacterial activity of foraging streptomycetes. (**A**) Bactericidal activity of foraging
604 streptomycetes determined by overlay-assays with indicator bacteria (Ec=*E. coli*, Bs=*Bacillus subtilis*)
605 on FAM, FAM+G and FAM+T. (**B**) Bactericidal activity of *S. coelicolor* developmental mutants as
606 determined by overlay assays on FAM. Dark purple indicates inhibition of indicator bacteria, light
607 purple indicates partial growth inhibition, and grey indicates that there was no detectable effect.

608 Figure supplement legends

609 **Figure 1 - figure supplement 1.** Nutrient levels during phenotype transition on 0.5xTSA. (**A**) The fold
610 change for every nutrient at every time point is plotted for both sampled positions on the dish. The
611 plot reveals a highly positive correlation, as indicated by the R-value of >0.96 suggesting a significant
612 linear relationship. (**B**) The fold change for each annotated metabolite during phenotype transition on
613 0.5xTSA is overlayed for both positions on the dish. The time point where the transition was observed
614 is indicated with the dotted lines at day 21. Source file of nutrient fold change over time in edge and
615 proximal samples used for the plots is available in the Figure 1 – Source data 2.

616 **Figure 2 - figure supplement 1.** Sector mutations of foraging colonies. Spores of *S. coelicolor* were
617 inoculated on FAM-agar and the sectors were isolated and subjected to Illumnia sequencing. The
618 inoculum was compared to the first level sector formed (α) and two succeeding sectors (I and IV)
619 originating from lineage α. Using the breseq software, two point mutations were detected in sector
620 α: DnaA (SCO3879:E520K) and uncharacterized DUF349-containing protein (SCO1511:+G). One
621 mutation was found in SCO5585 $(CG)_{5\rightarrow4}$ in linage IV.

622 **Figure 3 - figure supplement 1.** Secretome of foraging colonies. (**A**) Venn diagram of secretome from
623 nutrient deprived and rich conditions highlighting the shared and distinct protein profiles of each. (**B**)
624 PANTHER functional classification of proteins from the foraging secretomes that were predicted to
625 not have signal peptides. The plot shows the number of proteins assigned to each protein class.

626 **Figure 4 - figure supplement 1.** Growth of Streptomyces on FAM. (**A**) Growth of *S. coelicolor* wild-
627 types (M145 and M600) and developmental mutants: *bldA*, *whiA* (J2401), *whiB* (J2402), *whiG* (J2400),
628 *whiH* (J2408), *whiI* (J2450), and M851 (Δ*adpA*) on FAM. (**B**) Streptomycetes on FAM stained with lugol
629 solution after 5 days of incubation. Abbrevations: SANT; *S. antibioticus*, SANU; *S. anulatus*, SCO; *S.*
630 *coelicolor*, SFI; *S. filipinensis*, SGR; *S. griseus*, SGRI; *S. griseolus*, SHIR; *S. hiroshimensis*, SHYG; *S.*
631 *hygroscopicus*, SKAN; *S. kanamyceticus*, SLIV; *S. lividans*, SNOR; *S. norsei*, SVEN; *S. venezuelae*, KSET;
632 *Kitasatospora setae*. (**C**) Micrographs of the tested streptomycetes grown on FAM+G for 14 days. (**D**)
633 Micrographs of the tested streptomycetes grown on FAM+T for 14 days.

634 **Figure 5 – figure supplement 1.** Mold inhibition and significant unannotated metabolomic features.
635 (**A**) Inhibition of *P. citrinum by S. coelicolor* developmental mutants: *whiA* (J2401), *whiB* (J2402), *whiG*
636 (J2400), *whiH* (J2408), *whiI* (J2450) and wild-type M600. (**B**) Inhibition of local *Aspergillus*-isolate in an
637 overlay-assay on foraging S. coelicolor. Pictures were taken of foraging colonies using a dissection
638 microscope. (**C**) Plots of the unannotated metabolomic features unique to growth on FAM. The top
639 right corner of each graph indicates the molecular weight of corresponding metabolite. All graphs
640 depict statistically significant outcomes as determined by t-tests, with p-values <0.0001. Source file
641 with plotted values is available in the Figure 5 – figure supplement 1 - Source data 1.

642

643 ## References

644 A, J., Trygg, J., Gullberg, J., Johansson, A. I., Jonsson, P., Antti, H., . . . Moritz, T. (2005). Extraction and
645 GC/MS analysis of the human blood plasma metabolome. *Anal Chem, 77*(24), 8086-8094.
646 doi:10.1021/ac051211v
647 Barka, E. A., Vatsa, P., Sanchez, L., Gaveau-Vaillant, N., Jacquard, C., Meier-Kolthoff, J. P., . . . van
648 Wezel, G. P. (2016). Taxonomy, Physiology, and Natural Products of Actinobacteria.
649 *Microbiol Mol Biol Rev, 80*(1), 1-43. doi:10.1128/MMBR.00019-15
650 Bentley, S. D., Chater, K. F., Cerdeno-Tarraga, A. M., Challis, G. L., Thomson, N. R., James, K. D., . . .
651 Hopwood, D. A. (2002). Complete genome sequence of the model actinomycete
652 Streptomyces coelicolor A3(2). *Nature, 417*(6885), 141-147. doi:10.1038/417141a
653 Bibb, M. J. (2005). Regulation of secondary metabolism in streptomycetes. *Curr Opin Microbiol, 8*(2),
654 208-215. doi:10.1016/j.mib.2005.02.016

Bush, M. J., Tschowri, N., Schlimpert, S., Flardh, K., & Buttner, M. J. (2015). c-di-GMP signalling and the regulation of developmental transitions in streptomycetes. *Nat Rev Microbiol, 13*(12), 749-760. doi:10.1038/nrmicro3546

Chater, K. F., Biro, S., Lee, K. J., Palmer, T., & Schrempf, H. (2010). The complex extracellular biology of Streptomyces. *FEMS Microbiol Rev, 34*(2), 171-198. doi:10.1111/j.1574-6976.2009.00206.x

Chavez, A., Forero, A., Sanchez, M., Rodriguez-Sanoja, R., Mendoza-Hernandez, G., Servin-Gonzalez, L., . . . Sanchez, S. (2011). Interaction of SCO2127 with BldKB and its possible connection to carbon catabolite regulation of morphological differentiation in Streptomyces coelicolor. *Appl Microbiol Biotechnol, 89*(3), 799-806. doi:10.1007/s00253-010-2905-8

Datta, R., Baraniya, D., Wang, Y.-F., Kelkar, A., Meena, R. S., Yadav, G. S., . . . Formanek, P. (2017). Amino Acid: Its Dual Role as Nutrient and Scavenger of Free Radicals in Soil. *Sustainability, 9*(8), 1402. Retrieved from https://www.mdpi.com/2071-1050/9/8/1402

Deatherage, D. E., & Barrick, J. E. (2014). Identification of mutations in laboratory-evolved microbes from next-generation sequencing data using breseq. *Methods Mol Biol, 1151*, 165-188. doi:10.1007/978-1-4939-0554-6_12

Douglas, A. E. (2020). The microbial exometabolome: ecological resource and architect of microbial communities. *Philos Trans R Soc Lond B Biol Sci, 375*(1798), 20190250. doi:10.1098/rstb.2019.0250

Drula, E., Garron, M. L., Dogan, S., Lombard, V., Henrissat, B., & Terrapon, N. (2022). The carbohydrate-active enzyme database: functions and literature. *Nucleic Acids Res, 50*(D1), D571-D577. doi:10.1093/nar/gkab1045

Fink, D., Weissschuh, N., Reuther, J., Wohlleben, W., & Engels, A. (2002). Two transcriptional regulators GlnR and GlnRII are involved in regulation of nitrogen metabolism in Streptomyces coelicolor A3(2). *Mol Microbiol, 46*(2), 331-347. doi:10.1046/j.1365-2958.2002.03150.x

Flardh, K., & Buttner, M. J. (2009). Streptomyces morphogenetics: dissecting differentiation in a filamentous bacterium. *Nat Rev Microbiol, 7*(1), 36-49. doi:10.1038/nrmicro1968

Hobbs, G., Obanye, A. I., Petty, J., Mason, J. C., Barratt, E., Gardner, D. C., . . . Oliver, S. G. (1992). An integrated approach to studying regulation of production of the antibiotic methylenomycin by Streptomyces coelicolor A3(2). *J Bacteriol, 174*(5), 1487-1494. doi:10.1128/jb.174.5.1487-1494.1992

Hodgson, D. A. (2000). Primary metabolism and its control in streptomycetes: A most unusual group of bacteria. In *Advances in Microbial Physiology* (Vol. 42, pp. 47-238): Academic Press.

Ikeda, H., Ishikawa, J., Hanamoto, A., Shinose, M., Kikuchi, H., Shiba, T., . . . Omura, S. (2003). Complete genome sequence and comparative analysis of the industrial microorganism Streptomyces avermitilis. *Nat Biotechnol, 21*(5), 526-531. doi:10.1038/nbt820

Inselsbacher, E., & Nasholm, T. (2012). The below-ground perspective of forest plants: soil provides mainly organic nitrogen for plants and mycorrhizal fungi. *The New phytologist, 195*(2), 329-334. doi:10.1111/j.1469-8137.2012.04169.x

Inselsbacher, E., Öhlund, J., Jämtgård, S., Huss-Danell, K., & Näsholm, T. (2011). The potential of microdialysis to monitor organic and inorganic nitrogen compounds in soil. *Soil biology & biochemistry, 43*(6), 1321-1332. doi:10.1016/j.soilbio.2011.03.003

Jain, C., Rodriguez, R. L., Phillippy, A. M., Konstantinidis, K. T., & Aluru, S. (2018). High throughput ANI analysis of 90K prokaryotic genomes reveals clear species boundaries. *Nat Commun, 9*(1), 5114. doi:10.1038/s41467-018-07641-9

Jones, D. L., & Murphy, D. V. (2007). Microbial response time to sugar and amino acid additions to soil. *Soil biology & biochemistry, 39*(8), 2178-2182. doi:10.1016/j.soilbio.2007.03.017

Jones, S. E., Ho, L., Rees, C. A., Hill, J. E., Nodwell, J. R., & Elliot, M. A. (2017). Streptomyces exploration is triggered by fungal interactions and volatile signals. *Elife, 6*. doi:10.7554/eLife.21738

Kieser, T., Bibb, M. J., Buttner, M. J., Chater, K. F., Hopwood, D. A., & John Innes, F. (2000). *Practical Streptomyces genetics*. Norwich: John Innes Foundation Norwich.

Kim, D. W., Chater, K. F., Lee, K. J., & Hesketh, A. (2005). Effects of growth phase and the developmentally significant bldA-specified tRNA on the membrane-associated proteome of Streptomyces coelicolor. *Microbiology (Reading), 151*(Pt 8), 2707-2720. doi:10.1099/mic.0.28000-0

Labeda, D. P., Dunlap, C. A., Rong, X., Huang, Y., Doroghazi, J. R., Ju, K. S., & Metcalf, W. W. (2017). Phylogenetic relationships in the family Streptomycetaceae using multi-locus sequence analysis. *Antonie Van Leeuwenhoek, 110*(4), 563-583. doi:10.1007/s10482-016-0824-0

Labeda, D. P., Goodfellow, M., Brown, R., Ward, A. C., Lanoot, B., Vanncanneyt, M., . . . Hatano, K. (2012). Phylogenetic study of the species within the family Streptomycetaceae. *Antonie Van Leeuwenhoek, 101*(1), 73-104. doi:10.1007/s10482-011-9656-0

Leitner, S., Minixhofer, P., Inselsbacher, E., Keiblinger, K. M., Zimmermann, M., & Zechmeister-Boltenstern, S. (2017). Short-term soil mineral and organic nitrogen fluxes during moderate and severe drying–rewetting events. *Applied soil ecology : a section of Agriculture, ecosystems & environment, 114*, 28-33. doi:10.1016/j.apsoil.2017.02.014

Liebermeister, W., Noor, E., Flamholz, A., Davidi, D., Bernhardt, J., & Milo, R. (2014). Visual account of protein investment in cellular functions. *Proc Natl Acad Sci U S A, 111*(23), 8488-8493. doi:10.1073/pnas.1314810111

Martin, J. F. (2004). Phosphate control of the biosynthesis of antibiotics and other secondary metabolites is mediated by the PhoR-PhoP system: an unfinished story. *J Bacteriol, 186*(16), 5197-5201. doi:10.1128/JB.186.16.5197-5201.2004

McCormick, J. R., & Flardh, K. (2012). Signals and regulators that govern Streptomyces development. *FEMS Microbiol Rev, 36*(1), 206-231. doi:10.1111/j.1574-6976.2011.00317.x

Miyamoto, S., Atsuyama, K., Ekino, K., & Shin, T. (2018). Estimating the Diffusion Coefficients of Sugars Using Diffusion Experiments in Agar-Gel and Computer Simulations. *Chem Pharm Bull (Tokyo), 66*(6), 632-636. doi:10.1248/cpb.c18-00071

Moumbock, A. F. A., Gao, M., Qaseem, A., Li, J., Kirchner, P. A., Ndingkokhar, B., . . . Gunther, S. (2021). StreptomeDB 3.0: an updated compendium of streptomycetes natural products. *Nucleic Acids Res, 49*(D1), D600-D604. doi:10.1093/nar/gkaa868

Nett, M., Ikeda, H., & Moore, B. S. (2009). Genomic basis for natural product biosynthetic diversity in the actinomycetes. *Nat Prod Rep, 26*(11), 1362-1384. doi:10.1039/b817069j

Nikolaidis, M., Hesketh, A., Frangou, N., Mossialos, D., Van de Peer, Y., Oliver, S. G., & Amoutzias, G. D. (2023). A panoramic view of the genomic landscape of the genus Streptomyces. *Microb Genom, 9*(6). doi:10.1099/mgen.0.001028

Nodwell, J. R., & Losick, R. (1998). Purification of an extracellular signaling molecule involved in production of aerial mycelium by Streptomyces coelicolor. *J Bacteriol, 180*(5), 1334-1337. doi:10.1128/JB.180.5.1334-1337.1998

Ochi, K., & Hosaka, T. (2013). New strategies for drug discovery: activation of silent or weakly expressed microbial gene clusters. *Appl Microbiol Biotechnol, 97*(1), 87-98. doi:10.1007/s00253-012-4551-9

Ohnishi, Y., Ishikawa, J., Hara, H., Suzuki, H., Ikenoya, M., Ikeda, H., . . . Horinouchi, S. (2008). Genome sequence of the streptomycin-producing microorganism Streptomyces griseus IFO 13350. *J Bacteriol, 190*(11), 4050-4060. doi:10.1128/JB.00204-08

Pinu, F. R., Granucci, N., Daniell, J., Han, T. L., Carneiro, S., Rocha, I., . . . Villas-Boas, S. G. (2018). Metabolite secretion in microorganisms: the theory of metabolic overflow put to the test. *Metabolomics, 14*(4), 43. doi:10.1007/s11306-018-1339-7

Qin, Z., Munnoch, J. T., Devine, R., Holmes, N. A., Seipke, R. F., Wilkinson, K. A., . . . Hutchings, M. I. (2017). Formicamycins, antibacterial polyketides produced by Streptomyces formicae isolated from African Tetraponera plant-ants. *Chem Sci, 8*(4), 3218-3227. doi:10.1039/c6sc04265a

Randewig, D., Marshall, J. D., Näsholm, T., & Jämtgård, S. (2019). Combining microdialysis with metabolomics to characterize the in situ composition of dissolved organic compounds in boreal forest soil. *Soil Biology and Biochemistry, 136*, 107530. doi:https://doi.org/10.1016/j.soilbio.2019.107530

Reuther, J., & Wohlleben, W. (2007). Nitrogen metabolism in Streptomyces coelicolor: transcriptional and post-translational regulation. *J Mol Microbiol Biotechnol, 12*(1-2), 139-146. doi:10.1159/000096469

Romero-Rodriguez, A., Rocha, D., Ruiz-Villafan, B., Guzman-Trampe, S., Maldonado-Carmona, N., Vazquez-Hernandez, M., . . . Sanchez, S. (2017). Carbon catabolite regulation in Streptomyces: new insights and lessons learned. *World J Microbiol Biotechnol, 33*(9), 162. doi:10.1007/s11274-017-2328-0

Rousk, J., & Jones, D. L. (2010). Loss of low molecular weight dissolved organic carbon (DOC) and nitrogen (DON) in H2O and 0.5 M K2SO4 soil extracts. *Soil biology & biochemistry, 42*(12), 2331-2335. doi:10.1016/j.soilbio.2010.08.017

Sanchez, S., Chavez, A., Forero, A., Garcia-Huante, Y., Romero, A., Sanchez, M., . . . Ruiz, B. (2010). Carbon source regulation of antibiotic production. *J Antibiot (Tokyo), 63*(8), 442-459. doi:10.1038/ja.2010.78

Schauer, N., Steinhauser, D., Strelkov, S., Schomburg, D., Allison, G., Moritz, T., . . . Kopka, J. (2005). GC-MS libraries for the rapid identification of metabolites in complex biological samples. *FEBS Lett, 579*(6), 1332-1337. doi:10.1016/j.febslet.2005.01.029

Schindelin, J., Arganda-Carreras, I., Frise, E., Kaynig, V., Longair, M., Pietzsch, T., . . . Cardona, A. (2012). Fiji: an open-source platform for biological-image analysis. *Nat Methods, 9*(7), 676-682. doi:10.1038/nmeth.2019

Shepherdson, E. M. F., & Elliot, M. A. (2022). Cryptic specialized metabolites drive Streptomyces exploration and provide a competitive advantage during growth with other microbes. *Proc Natl Acad Sci U S A, 119*(40), e2211052119. doi:10.1073/pnas.2211052119

Shevchenko, A., Tomas, H., Havlis, J., Olsen, J. V., & Mann, M. (2006). In-gel digestion for mass spectrometric characterization of proteins and proteomes. *Nat Protoc, 1*(6), 2856-2860. doi:10.1038/nprot.2006.468

Shirling, E. B., & Gottlieb, D. (1966). Methods for characterization of Streptomyces species. *International journal of systematic bacteriology, 16*(3), 313-340. doi:10.1099/00207713-16-3-313

Teufel, F., Almagro Armenteros, J. J., Johansen, A. R., Gislason, M. H., Pihl, S. I., Tsirigos, K. D., . . . Nielsen, H. (2022). SignalP 6.0 predicts all five types of signal peptides using protein language models. *Nat Biotechnol, 40*(7), 1023-1025. doi:10.1038/s41587-021-01156-3

van der Meij, A., Worsley, S. F., Hutchings, M. I., & van Wezel, G. P. (2017). Chemical ecology of antibiotic production by actinomycetes. *FEMS Microbiol Rev, 41*(3), 392-416. doi:10.1093/femsre/fux005

van Keulen, G., & Dyson, P. J. (2014). Production of Specialized Metabolites by Streptomyces coelicolor A3(2). *Advances in Applied Microbiology, 89*, 217-266. doi:10.1016/B978-0-12-800259-9.00006-8

Widdick, D. A., Dilks, K., Chandra, G., Bottrill, A., Naldrett, M., Pohlschroder, M., & Palmer, T. (2006). The twin-arginine translocation pathway is a major route of protein export in Streptomyces coelicolor. *Proc Natl Acad Sci U S A, 103*(47), 17927-17932. doi:10.1073/pnas.0607025103

Zhang, X., Hindra, & Elliot, M. A. (2019). Unlocking the trove of metabolic treasures: activating silent biosynthetic gene clusters in bacteria and fungi. *Curr Opin Microbiol, 51*, 9-15. doi:10.1016/j.mib.2019.03.003

Zhang, Z., Du, C., de Barsy, F., Liem, M., Liakopoulos, A., van Wezel, G. P., . . . Rozen, D. E. (2020). Antibiotic production in Streptomyces is organized by a division of labor through terminal genomic differentiation. *Sci Adv, 6*(3), eaay5781. doi:10.1126/sciadv.aay5781

Figure 1. *S. coelicolor* growth phenotype transition correlates with nutrient depletion.

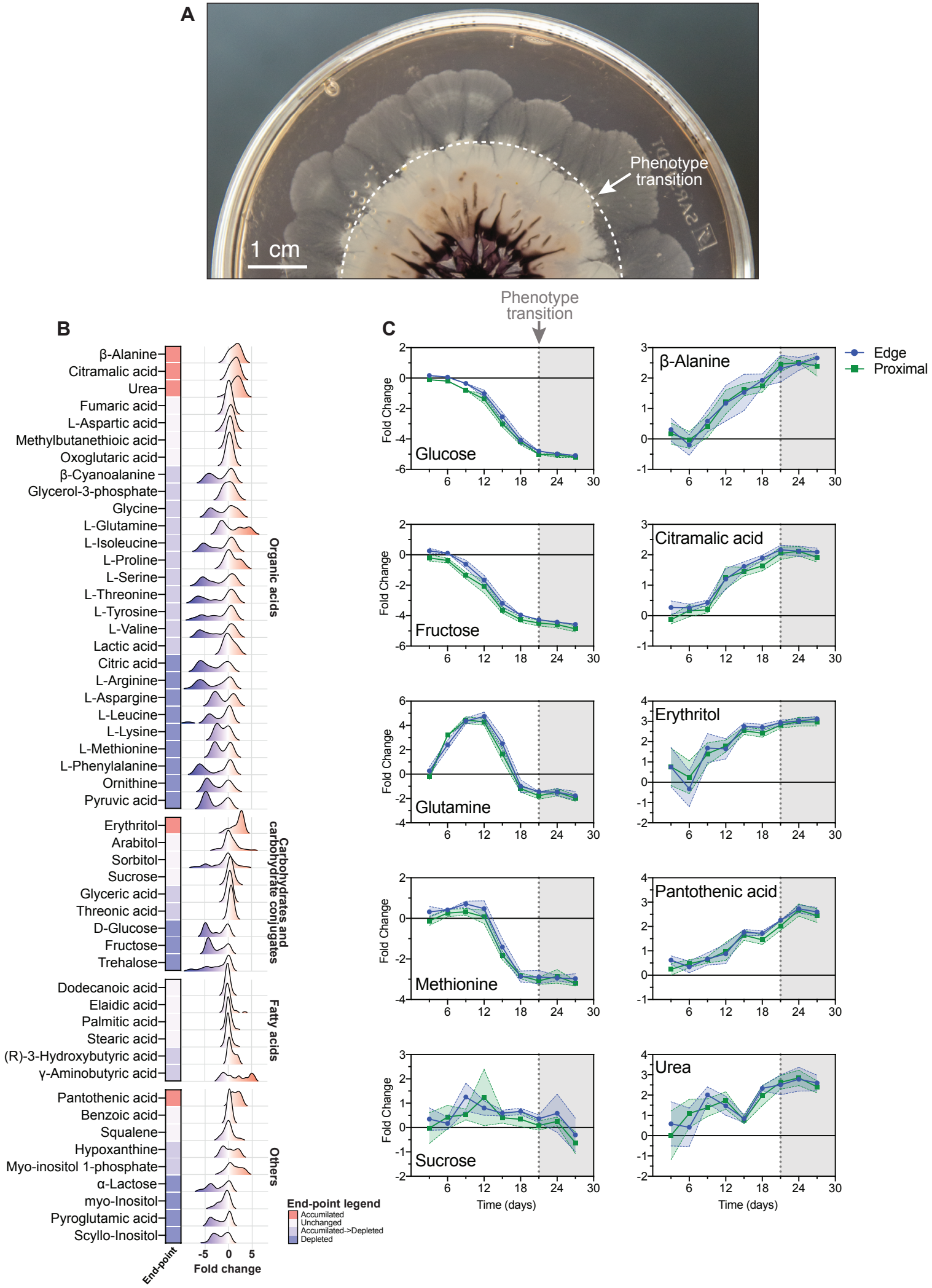

Figure 2. Nutrient poor agar media promote the *S. coelicolor* foraging phenotype.

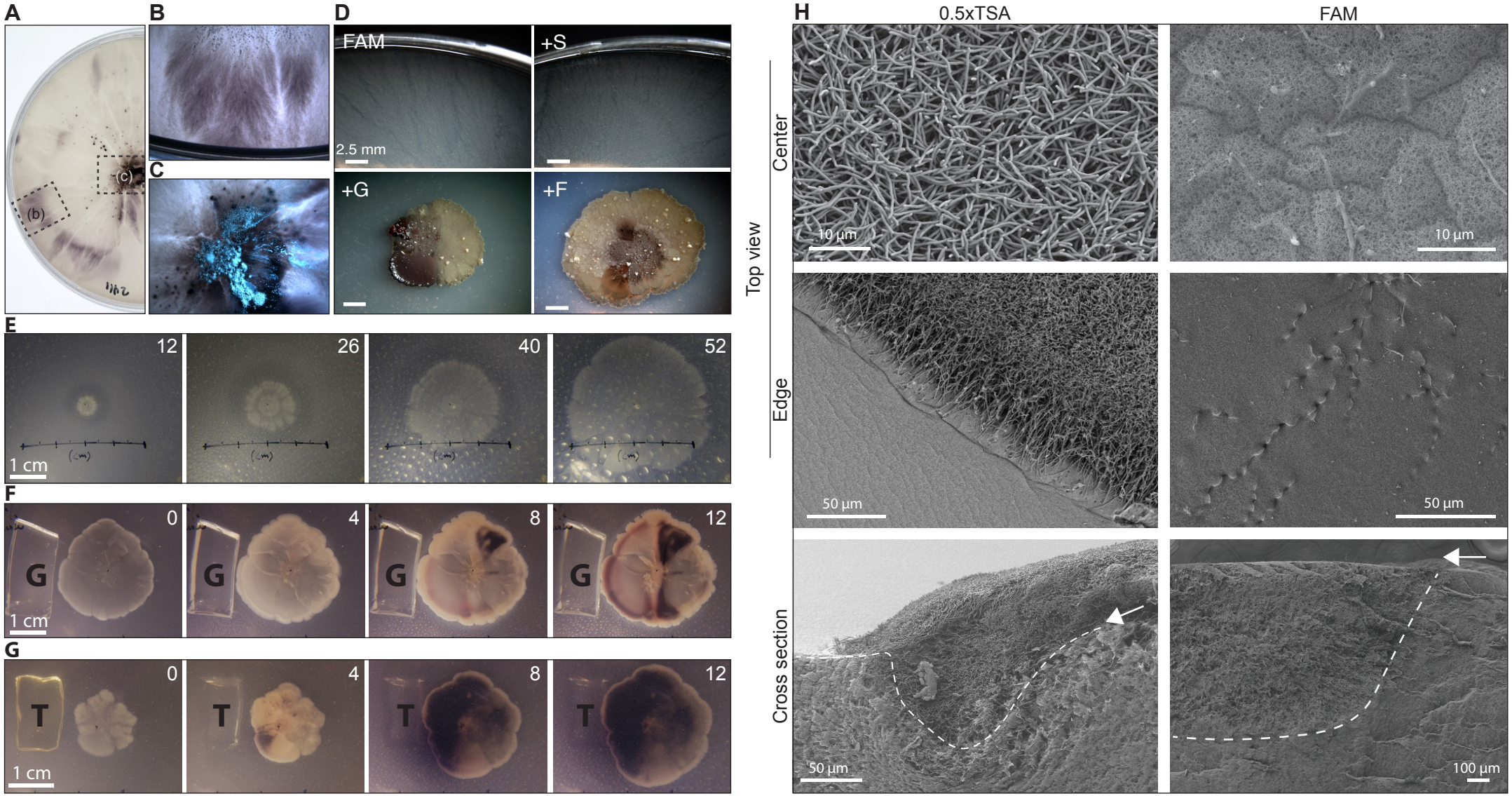

Figure 3. Characterization of the foraging phenotype secretome.

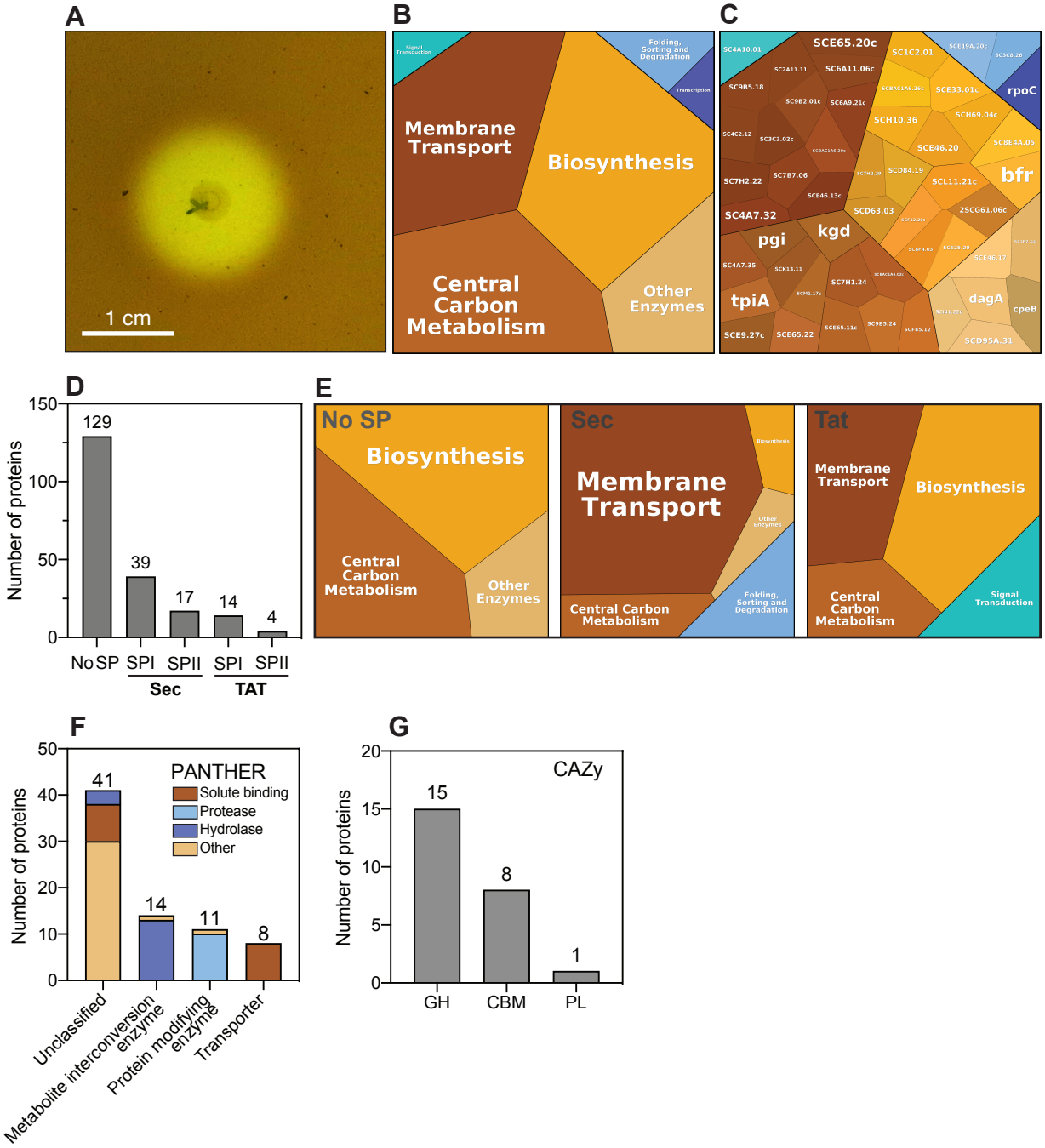

Figure 4. Phylogenetically separated streptomycetes display the foraging phenotype.

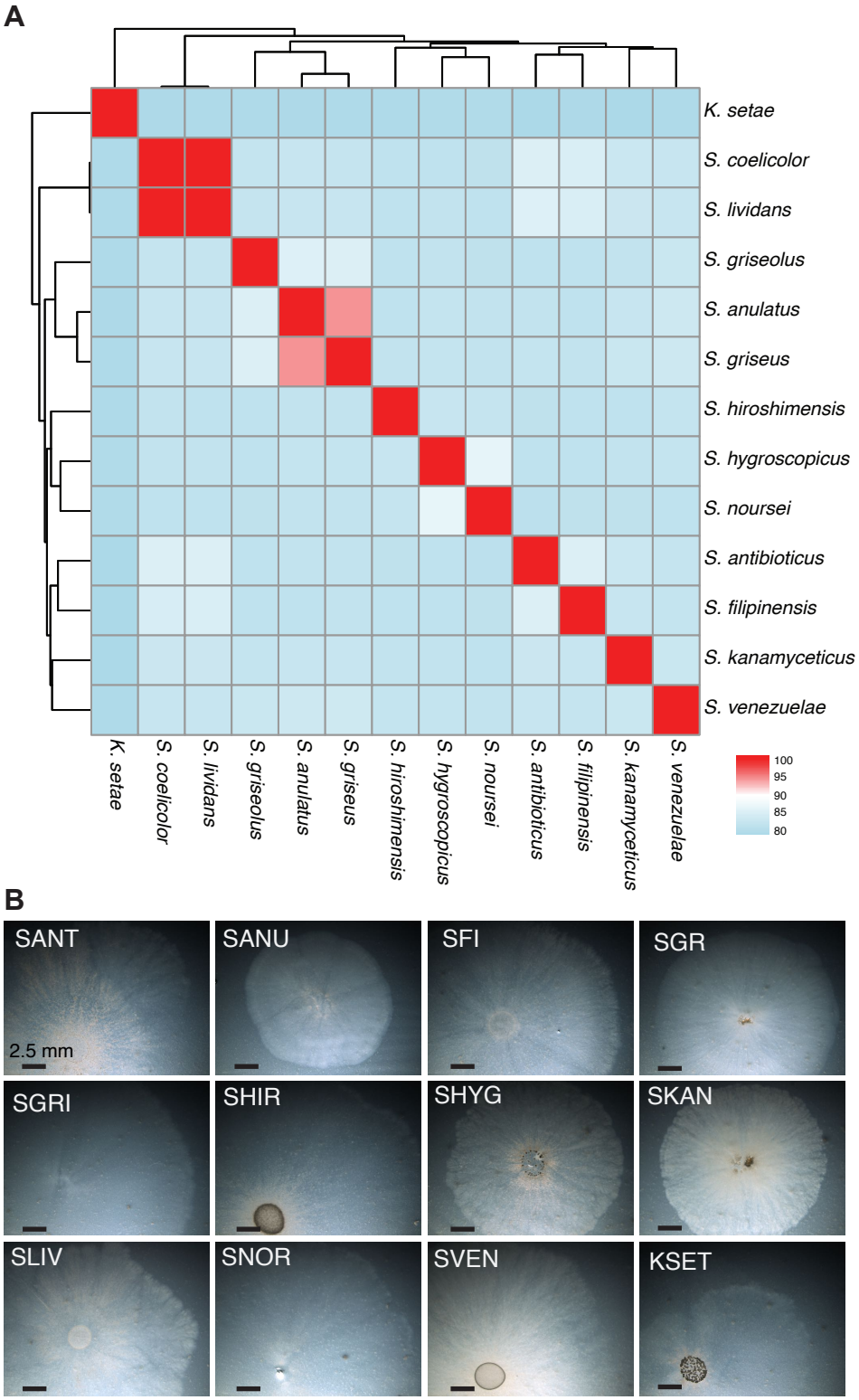

Figure 5. Mold inhibitory activity and metabolomic analysis of foraging *S. coelicolor*.

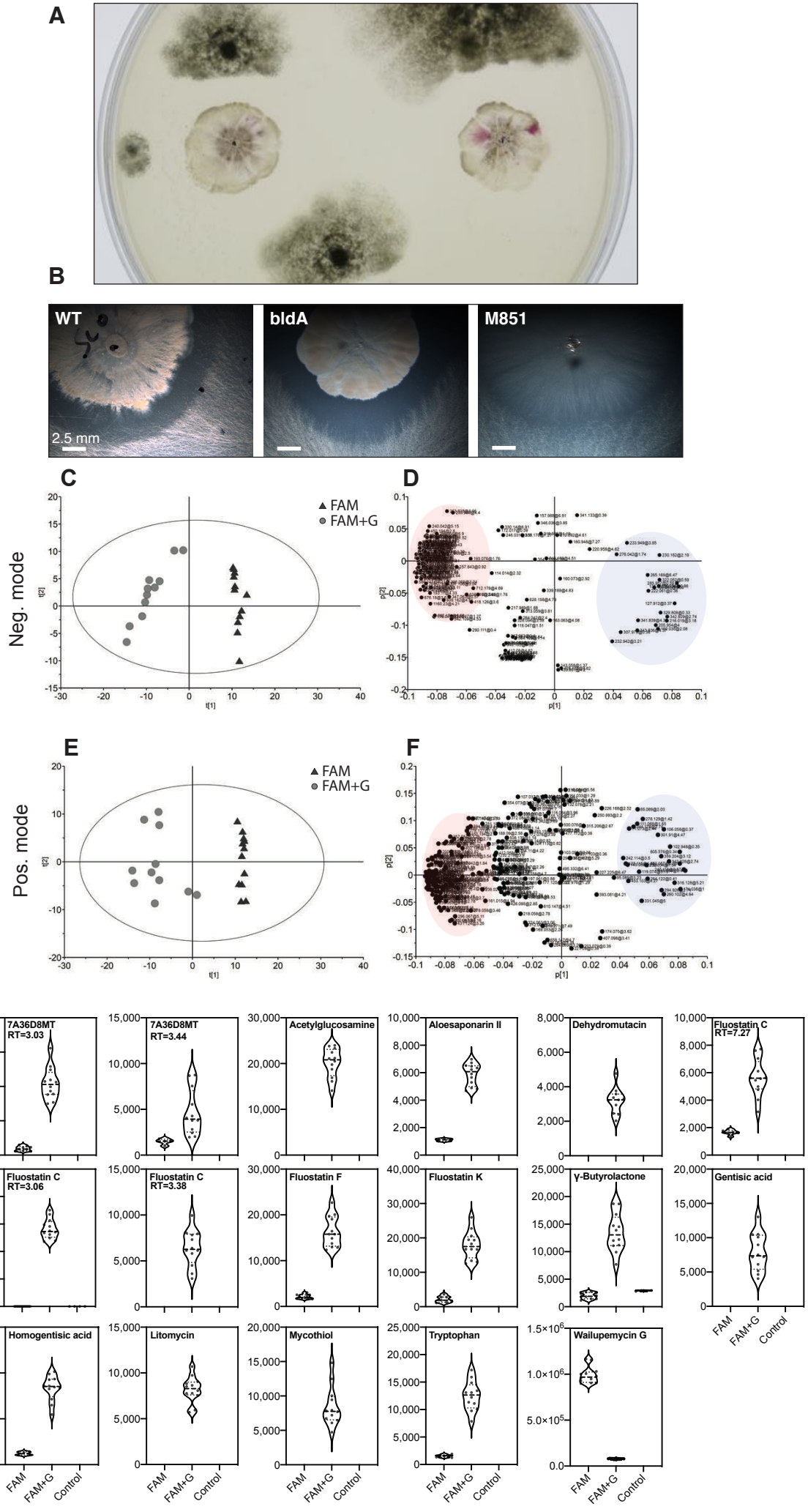

Figure 6. Antibacterial activity of foraging streptomycetes.

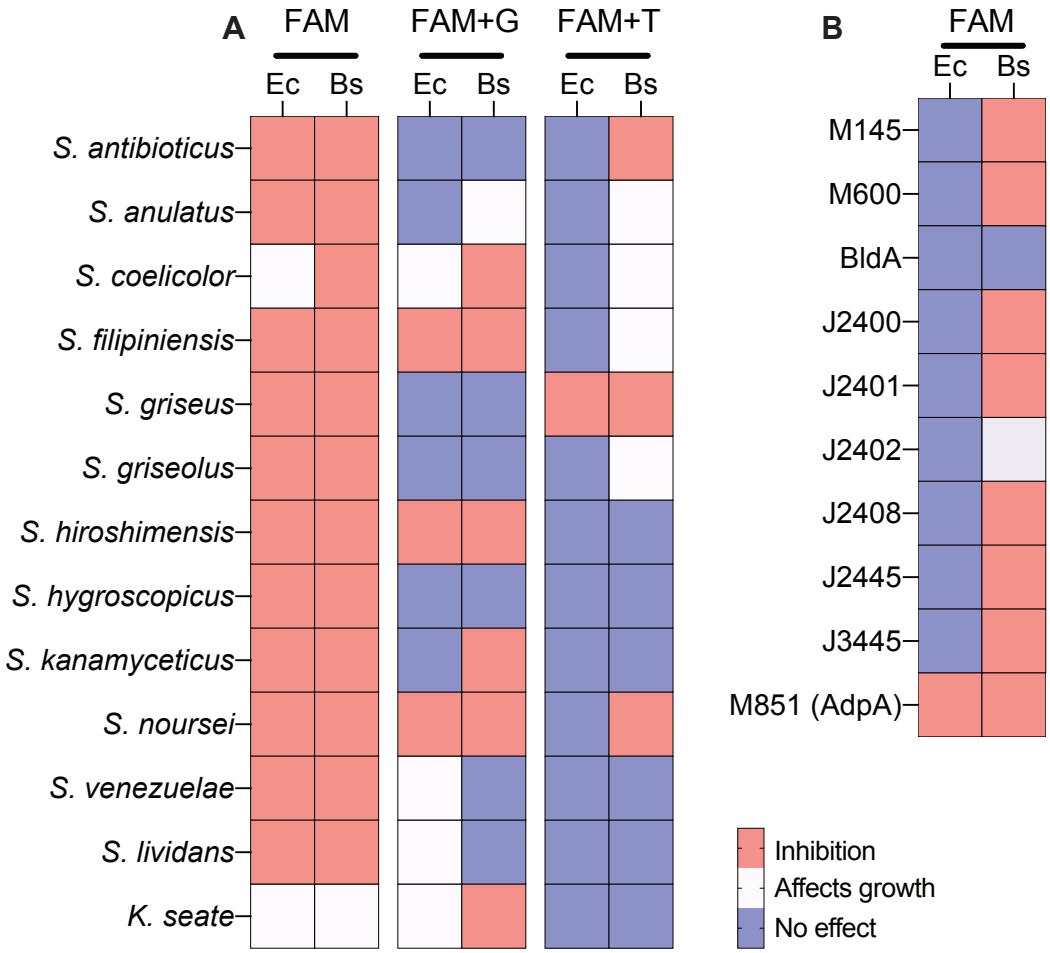

Figure 1 - figure supplement 1

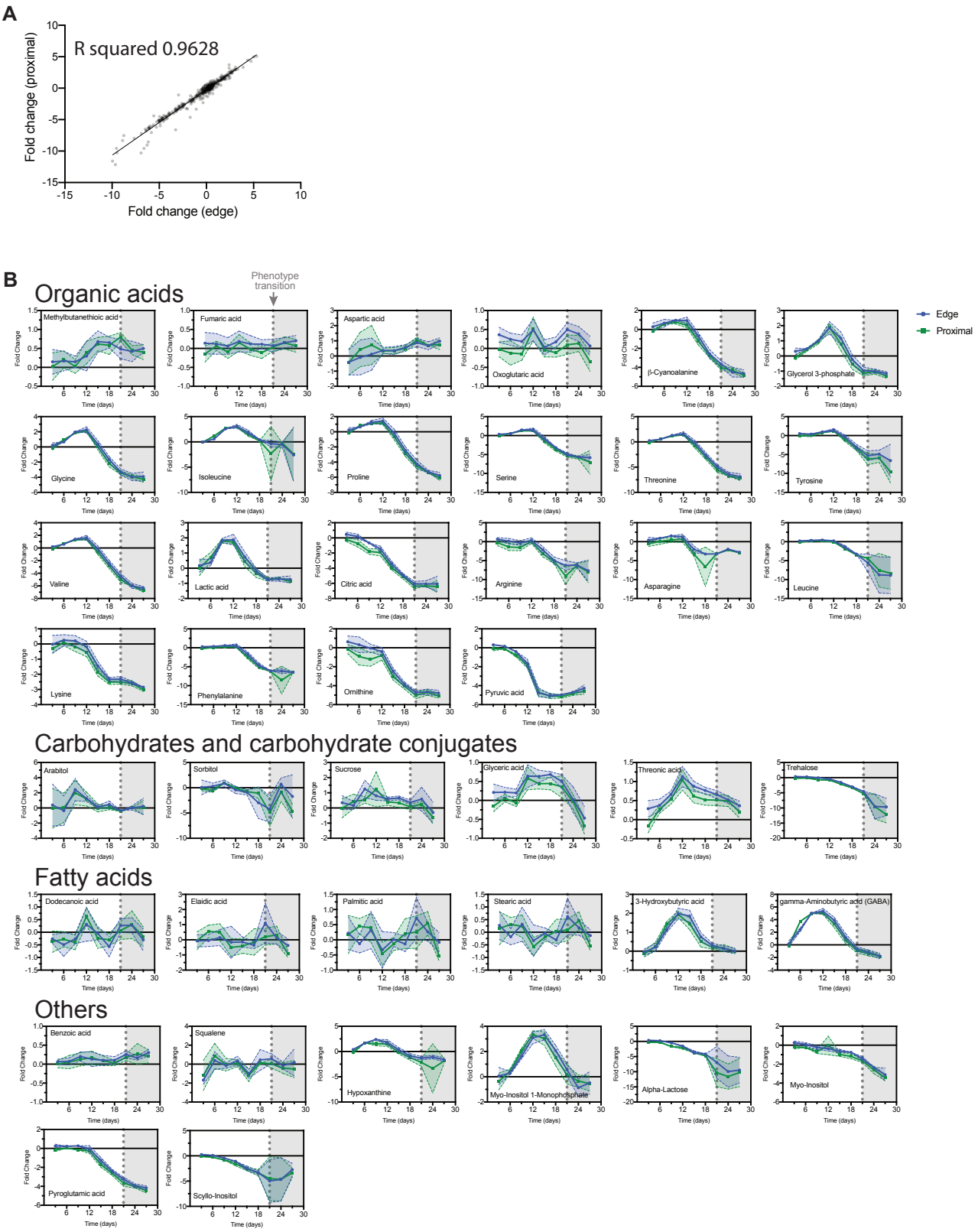

Figure 2 - figure supplement 1

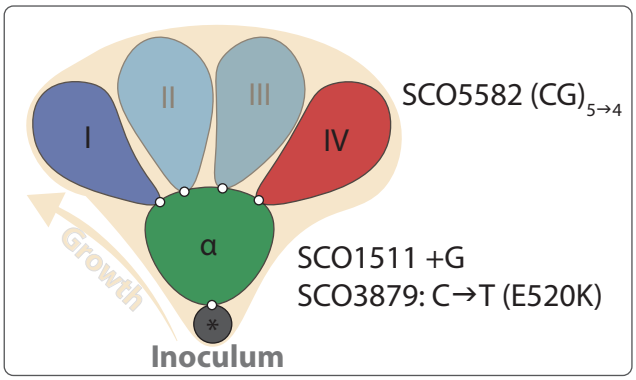

→!

Figure 3 - figure supplement 1

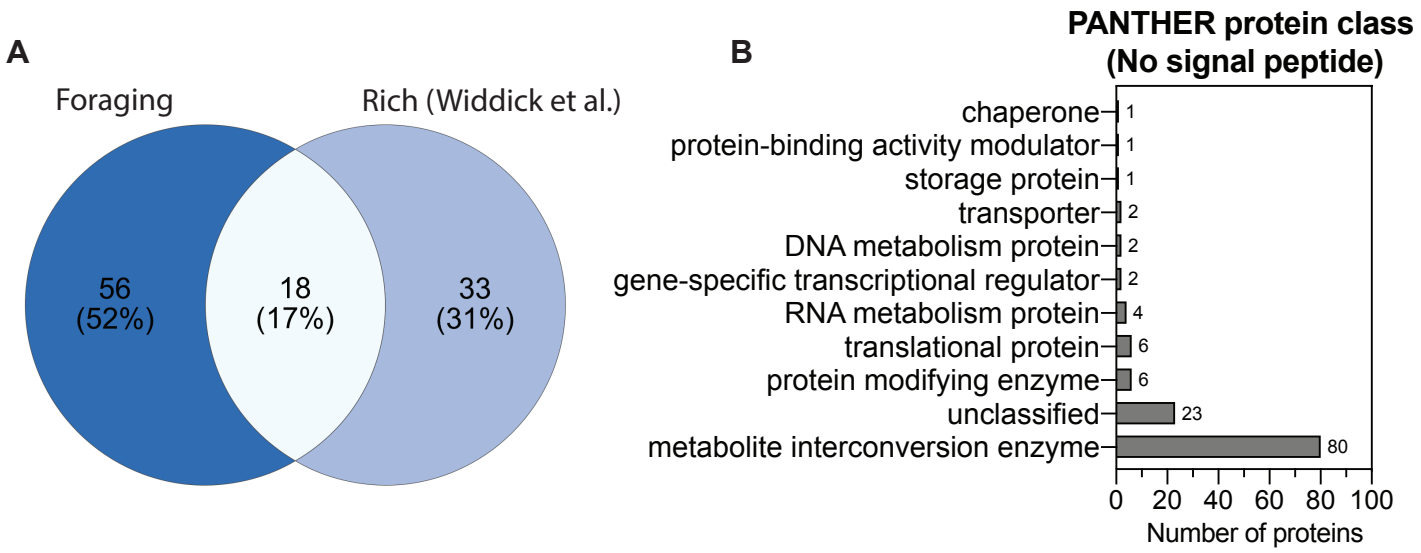

Figure 4 - figure supplement 1

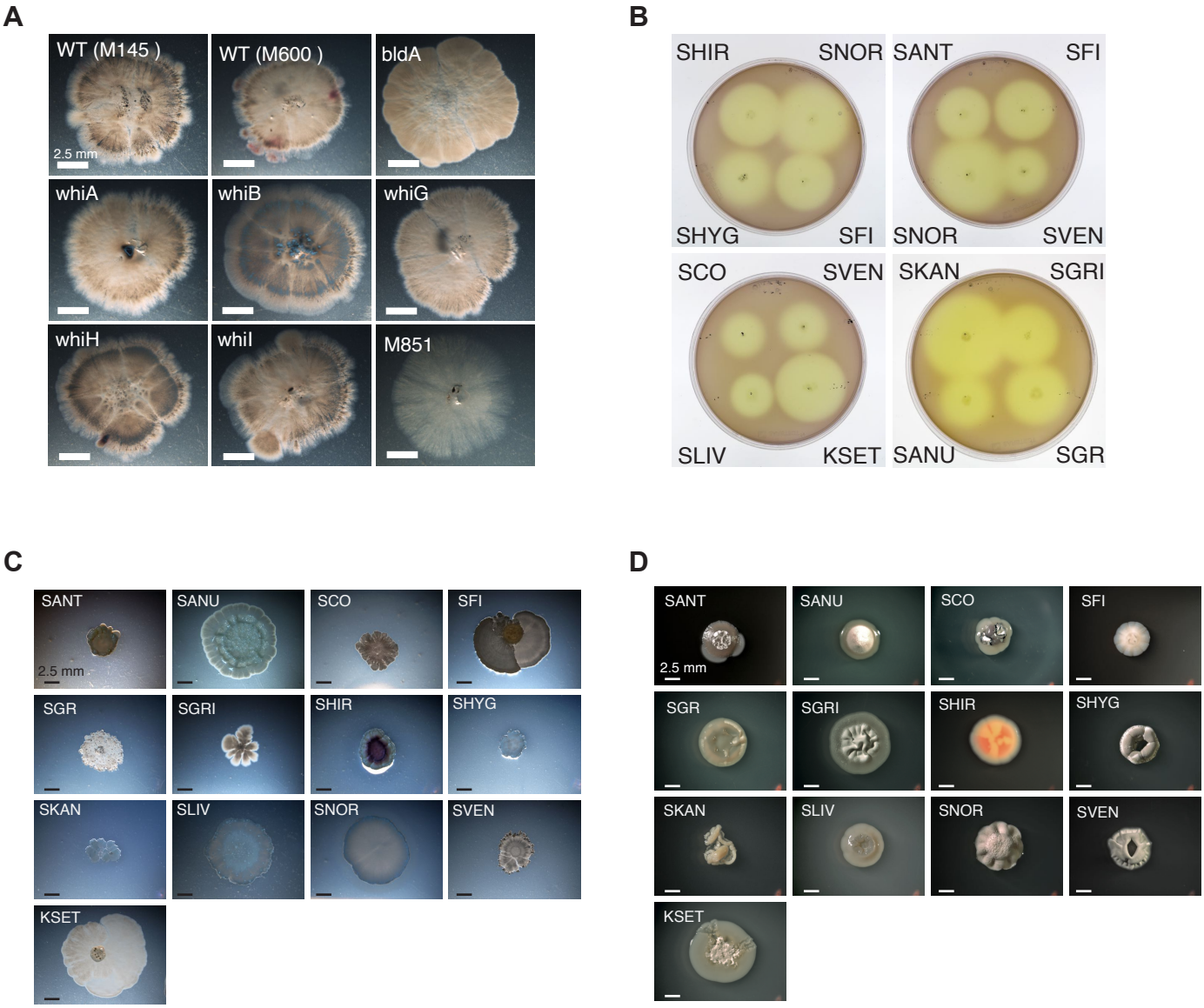
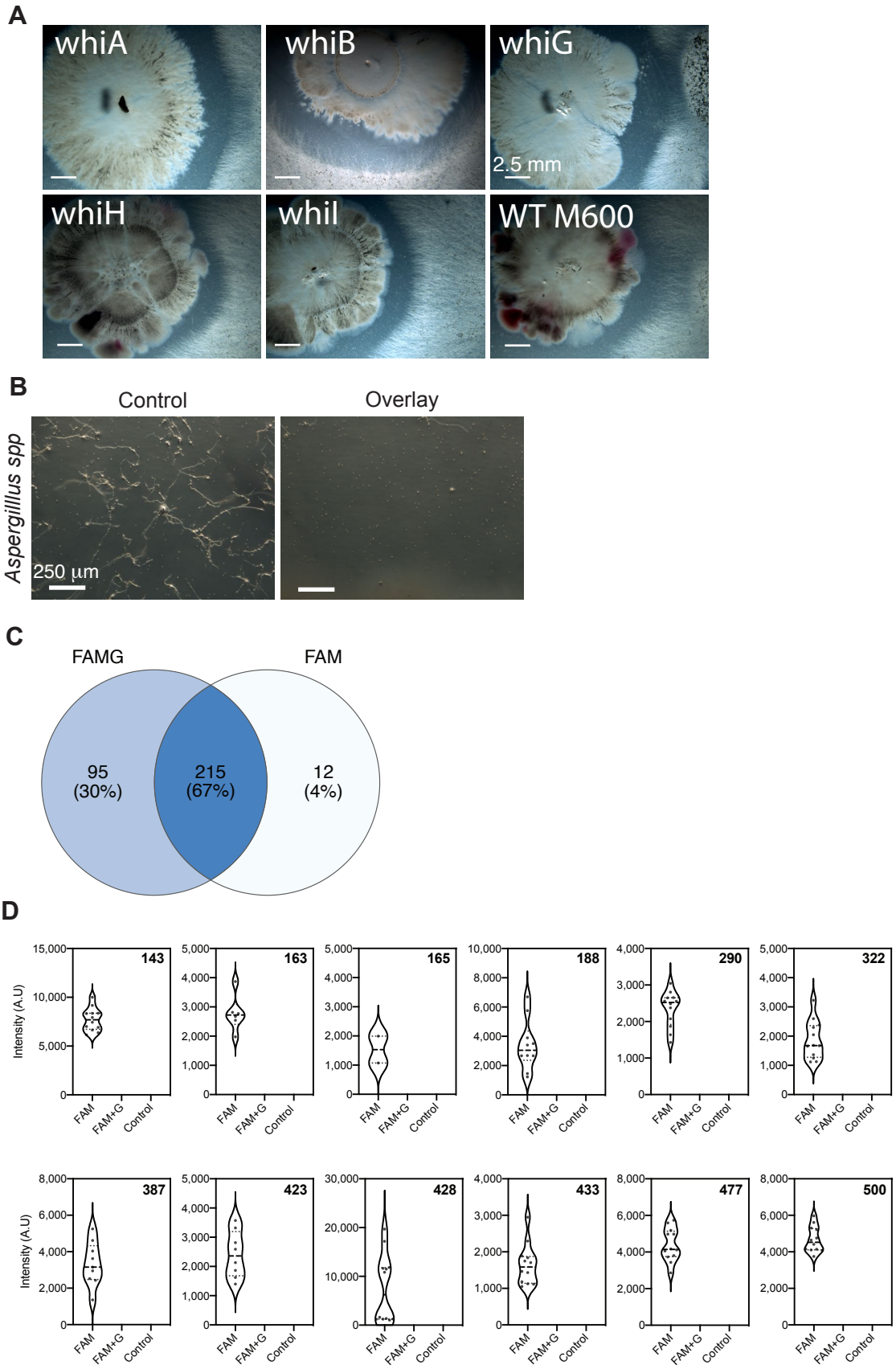
Figure 5 - figure supplement 1